Journal of Applied Research in Water and Wastewater
E-ISSN: 2476-6283
Journal homepage: https://arww.razi.ac.ir

Comparative evaluation of CFD model and intelligence hybrid method to ameliorate ANFIS in side weir coefficient of discharge modelling

Mohammadmehdi Razmi[1], Mojtaba Saneie[1,2,3*], Shamsa Basirat[1]

[1]Department of Civil Engineering, Najafabad Branch, Islamic Azad University, Najafabad, Iran.
[2]Soil Conservation and Watershed Management Research Institute, (SCWMRI), Tehran, Iran.
[3]Agricultural Research, Education and Extension Organization (AREEO), Tehran, Iran.

GRAPHICAL ABSTRACT

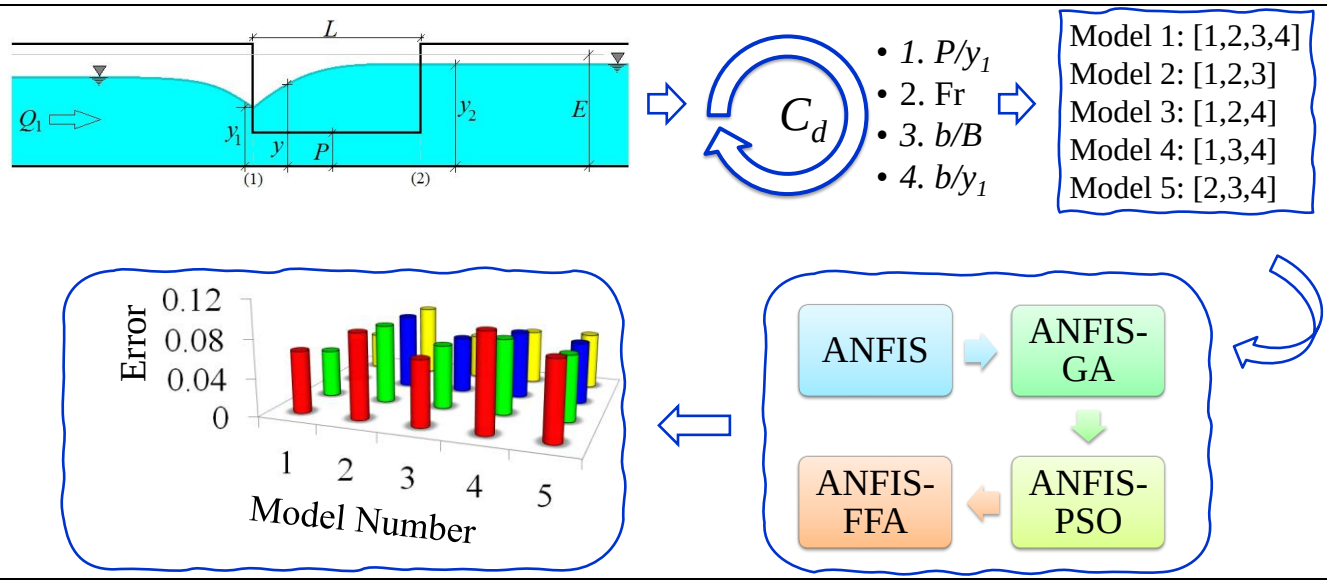

ARTICLE INFO

Article history:
Received 2 July 2022
Reviewed 15 September 2022
Received in revised form 3 November 2022
Accepted 7 November 2022
Available online 10 November 2022

Keywords:
Computational fluid dynamics
Discharge coefficient
Firefly algorithm
Neuro-fuzzy systems
Sensitivity analysis
Side weir

Article type: Research Article

ABSTRACT

In this paper, the ANFIS network was optimized using three algorithms comprising the Particle Swarm Optimization (PSO), Firefly Algorithm (FFA), and Genetic algorithm (GA) for the first time. To ameliorate the ability of the numerical models, the Monte Carlo simulations were utilized. Moreover, in order to assess the simulation outcomes, the k-fold cross validation technique was implemented. Initially, using all inputs, five different parameters were used for producing the ANFIS, ANFIS-GA, ANFIS-PSO, and ANFIS-FFA methods. After that, a computational fluid dynamics (CFD) model simulated the discharge coefficient (DC) and the outcome of all simulations were compared. The analysis of the results demonstrated that the ANFIS-FFA model approximates the DC with higher precision. For instance, the amount of the coefficient of determination and the scatter index were surmised as 0.961 and 0.039. Also, the side weir height ratio to the upstream depth (P/y1) was detected as the most influential parameter. About 85% of the DC simulated by the ANFIS-FFA model had an inaccuracy of less than 5%. The performed uncertainty analysis proved that the best model possesses an underestimated efficiency. For this model, the influence of the inputs were analyzed in a ±10% range. Finally, a computational code was presented for the simulation of DC by hydraulic and environmental engineers.

1. Introduction

Generally, the discharge coefficient (DC) is a significant variable for designing side weirs. In addition, a side weir is located on main channels to divert exceeded flows. This sort of hydraulic structure is broadly employed in transmission channels and irrigation-drainage systems. The water at the situation of this diversion structure is completely three-dimensional and its simulation is crucially important. Thus, providing an optimized approach for the DC simulation is essential. Owing to complex structure of the water along with the side weir, numerous works have been implemented to model the hydraulics of this type of structures. Some researches have been devoted to experimentally investigate the hydraulics of side weirs (Ameri et al. 2016; Crispino et al. 2015; Emiroglu et al. 2017; Granata et al. 2016; Karimi et al. 2018; Khameneh et al. 2014; Novak et al. 2012; Onen et al. 2013; Paris et al. 2012; Zahiri et al. 2013).

CFD models are very accurate and cost-effective and require less time to run. Recently, CFD models have been utilized to simulate the

*Corresponding author Email: Saneie_m@scwmri.ac.ir

How to cite: M. Razmi, M. Saneie, S. Basirat, Comparative evaluation of CFD model and intelligence hybrid method to ameliorate ANFIS in side weir coefficient of discharge modelling, *Journal of Applied Research in Water and Wastewater*, 9 (2), 2022, 125-140.

flow field of side weirs (Abdollahi et al. 2017; Aydin et al. 2013; Aydin et al. 2015; Aydin 2015; Aydin and Emiroglu. 2016; Azimi et al. 2014; Azimi and Shabanlou. 2015; Azimi and Shabanlou 2018; Mahmodinia et al 2014). Several AI algorithms like artificial neural networks (ANNs), gene expression programming (GEP), Adaptive-Neuro Fuzzy Inference System (ANFIS) and Group Method of Data Handling (GMDH) are utilized for modeling various phenomena. Azamathulla et al. 2016; Azimi et al. 2017; Bagheri et al 2014; Chatterjee et al. 2022; Dursun et al. 2012; Ebtehaj et al. 2015; Emiroglu et al. 2011; Freitas et al. 2021; Ferreira et al. 2021; Khoshbin et al. 2016; Kisi et al 2012; Parsaie and Haghiabi. 2015; Roushangar et al. 2016; Sai et al. 2020 successfully predict side weirs DC utilizing different AI models. In addition, a group of scientists employed various methods such as CFD, analytical and artificial intelligence to examine the water and the DC. For example, Aydin 2016 compared the free surface alongside the weir estimated by the De Marchi method and the FLUENT software. Azimi et al. 2017 predicted the DC of orifices by a CFD model. They compared the CFD performance, ANFIS ,and ANFIS-Genetic Algorithm models and proved that ANFIS-GA acts more accurate in simulating the DC. Shafiei et al. 2020 used a CFD and a Fuzzy-based algorithm in predicting the DC of labyrinth weir.They compared the results obtained by the CFD model with the Fuzzy-based models and proved that ANFIS-FFA model was significantly more efficient.

In general, meta-heuristic algorithms by inspiration from natural mechanisms such as the movement of insects and the evolution of living organisms can optimize AI models and significantly increase the accuracy of modeling. Furthermore, optimization algorithms are significant aspects in this domain of soft computations which are increasingly used. For example, Genetic Algorithm (GA), Ant Colony Optimization(ACO), Particle Swarm Optimization(PSO), and Cuckoo Search(CS), are some of the meta-heuristic optimization algorithms which enhance the performance of artificial intelligence models by inspiring from various natural phenomena and optimize them. Furthermore, an optimization algorithm entitled "firefly algorithm" recently developed based on the advanced swarm theory and used by many researchers researchers (Azimi et al. 2018a; Ebtehaj and Bonakdari. 2016; Ebtehaj et al. 2017). This method emulates the behavior of firefly in nature which is associated with lighting. In other words, fireflies operate on the basis of blinking characteristics including brightness, frequency, and time. The firefly algorithm performs better in the global and local optimization than other algorithms.

The ANFIS network possesses a logical performance in simulating different phenomena compared to other AI models. Furthermore, different algorithms have been implemented for optimizing ANFIS. In the present work, for the first time, a modern meta-heuristic algorithm is developed using the firefly optimization algorithm and ANFIS for the estimation of the DC. Moreover, the performance of other optimization algorithms like GA and PSO are examined and compared with the firefly algorithm. To this end, utilizing the inputs, five distinct models are produces for each of the ANFIS, ANFIS-GA, ANFIS-PSO, and ANFIS-FFA models. In the current investigation, the Monte Carlo simulation (MCs) and the k-fold cross-validation technique are employed to increase the performance of the numerical models and verify the modeling results, respectively. In the following, the DC is simulated by CFD and compared with the AI models. After that, the best methodology and the most influential input parameter are identified, and the performance of the premium model is evaluated by conducting an uncertainty analysis. Finally, a code is presented for estimating the DC by engineers. As the novelty of the current study, the DC of side weirs was simultaneously simulated using three hybrid metaheuristic machine learning (HMML) algorithms and a CFD for the first time. The findings proved that the HMML had better performance to model the target parameter. DC Prediction of the rectangular side weirs by using several HMML algorithms and CFD model is the most important aim of the current work; however, assessment of the flow field such as contours or vectors of velocity is out of scope of this study.

2. Material and Methodology

2.1. Experimental model

In the present work, the experimental measurements obtained by Bagheri et al. 2014 were employed for verifying the outcomes of the numerical models. The laboratory apparatus is consist of an open conduit with a length of 8m and a side weir located at a 4.5m distance from the main channel inlet.

The width of the major conduit is 0.4 and the height is 0.6 and the main canal is horizontal. As shown in Fig. 1 a slide gate is installed to adjust the water in the major canal. Also, the limit of the measurements applied for verifying the simulation results is summarized in Table 1.

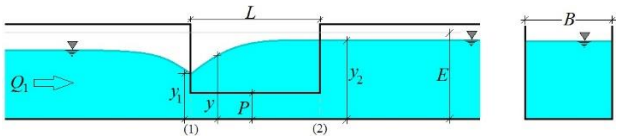

Fig. 1. Layout of laboratory model.

Table 1. Range of experimental results used for verifying results of numerical models.

	Maximum	Minimum	Average	Standard division	Variance
F_1	0.804	0.088	0.369	0.164	0.027
b/B	1.513	0.300	0.948	0.504	0.254
b/y_1	6.554	0.347	2.268	1.446	2.091
P/y_1	0.910	0.181	0.645	0.182	0.009
C_d	0.846	0.281	0.487	0.097	0.009

2.2. Discharge coefficient of side weir

Emiroglu et al. 2011 mentioned that the DC of side weirs is in terms of the upstream Froude number of the side weir (Fr), the side weir length to the main channel width ratio (*b/B*), the side weir length to the flow depth ratio (b/y_1), the height of the crest ratio (P/y_1), the diversion angle of the flow (ψ), and the bed slope of the major conduit (S_0) (Azimi et al. 2017):

$$C_d = f\left(\mathrm{Fr} = \frac{u}{\sqrt{gD}}, \frac{b}{B}, \frac{b}{y_1}, \frac{P}{y_1}, \psi, S_0\right) \quad (1)$$

The influence of ψ on the DC is hidden in the dimensionless parameters *b/B*. Also, the influence of ψ on the DC has not been assessed in the previous studies. Furthermore, Borghei et al. (1999) expressed that the channel bed slope effects (S_0) in subcritical flow conditions are negligible, so we have (Azimi et al. 2017):

$$C_d = f\left(\mathrm{Fr}, \frac{b}{B}, \frac{b}{y_1}, \frac{P}{y_1}\right) \quad (2)$$

Therefore, in the following, the factors of Eq. 2 are used for the simulation of DC. The input combinations for defining the Fuzzy-based models are illustrate in Fig. 2.

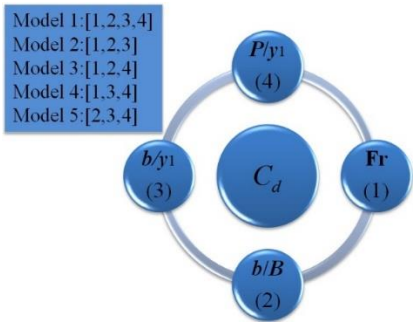

Fig. 2. Input parameters combinations for developing artificial intelligence models.

At this work, the Monte Carlo simulations (MCs) are utilized for enhancing the capability of the Fuzzy-based models. The MCs refers to any method providing rough results for quantitative problems through statistical prototyping. The MCs are mainly utilized for describing a method to distribute uncertainties existing in the model input to uncertainties of the model output. Thus, MCs is a simulation procedure exhibiting uncertainty explicitly and quantitatively. The MCs relies on the procedure of explicitly displaying an uncertainty by determining inputs as probability distributions. If the intakes describing a technique are non-deterministic, then the prediction of forwarding performance is necessarily probabilistic. This means that the outcome of any study established on intakes represented by likelihood distributions is a likelihood distribution itself. In the MCS, the entire procedure conducts multiple times (for example, 1000 times). Each simulation is named the realization of the method. For single realization, all unconfident variables are tested (i.e. an incidental matter of the typical allocation for each variables is chosen). Subsequently, this method is acted over time (with several inputs) so that the implementation of the method can be estimated. It outcomes in a considerable numeral of independent and independent outcomes so that each of them shows a potential next for the method. The outcomes

of independent realizations of the method will come in the form of possible distributions of potential results. Hence, results are not in the formation of single values, they are as an allocation of likelihoods. Likewise, The k-fold cross-validation (KFCV) procedure is operated to assess the noted examples' interpretation. The standard evaluation technique decides the scope to which the outcomes of statistical examination on a data set are generalizable and independent of educational data. This technique is especially utilized in foretelling applications to decide how beneficial the standard will truly be. In general, one round of the KFCV consists of splitting the data into two complementary subsets including acting accounting on one of those subsets (training data) and validating the computation using other set data (testing data). To decrease the distribution, the validation procedure is executed several times with various sub-samples and the verification outcomes are averaged. In the current work, k is considered to be equal to 5. Additionally, the schematic of the KFCV procedure and it's dealing with test and train data are displayed in Fig. 3.

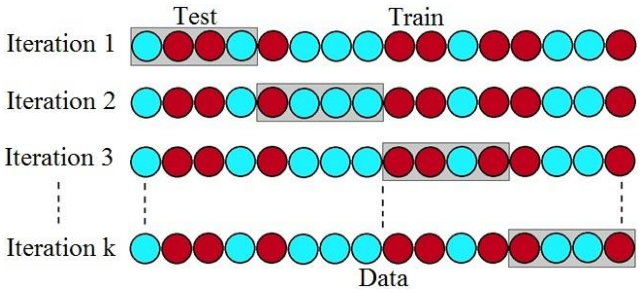

Fig. 3. k-fold cross-validation dealing with observational data.

2.3. Adaptive Neuro-Fuzzy Inference System (ANFIS)

ANFIS (Jang 1993) is a framework based on the integration of the Nero-Fuzzy and neural network (NN). To investigate the ANFIS architecture, an algorithm with two inputs(x_1 and x_2) considering Takagi-Sugeno if-then fuzzy part and the output y are determined as below:

Rule1:*if* (x_1 is A_1) and (x_2 is B_1) then $f_1 = p_1 x_1 + q_1 x_2 + r_1$

Rule2: *if* (x_1 is A_2) and (x_2 is B_2) then $f_2 = p_2 x_1 + q_2 x_2 + r_2$

Here, AandB are fuzzy parts, {p,q,r} are the subsequent parameters tuned using training mode. The ANFIS system is a network with 5 different layers. The initial layer involves fuzzy set input parameters so that all nodes are adapted to a function. Due to the suitable performance in different studies (Parsaie et al. 2017), the Gaussian principle is applied as the membership function (MF). The memberships of two members considered with two inputs in a fuzzy system are multiplied in each other in the second layer. In fact, fuzzy rules are expressed in the form of outcome. Neurons of the third layer that are non-adaptive or fix, exhibit the single input membership degree. The outcome of single node is estimated in the fourth layer. Neurons of this layer are adaptive. The fifth layer that only has a non-adaptive neuron estimates and provides the network outcome regarding the input signals from nodes belonging to layer1 to layer4. The structure of the ANFIS architecture is drawn in Fig. 4.

For modeling by ANFIS, the number of iterations is considered 2000. The optimized amount of the variable is calculated in the trial and error procedure so that by considering values, 500-3000 the model performance is studied and it is seen that enhancing the number of repetitions by greater than 2000 does not own a remarkable impact on the outcomes. Moreover, the optimal amount of initial increase, step-sizes decrease, and initial step sizes are opted as 1.15, 0.9, and 0.01. Furthermore, the fuzzy c-mean clustering (FCM) method known as a good approach for the fuzzy inference system (FIS) generation (Abdulshahed et al. 2015; Gholami et al. 2018; Yaseen et al. 2017; Yaseen et al. 2018) is utilized.

2.4. Application of Genetic Algorithm (GA) for training ANFIS

The GA is a revolutionary algorithm proposed (Goldberg and Holland 1988). The most significant advantage of this algorithm is its ability in global searching which is independent form problem situations and has an acceptable performance in solving complex problems. In addition to these problems, the trap in the local minimum problem, as one of the common problems in optimization problems, is not present in this algorithm (Shihabudheen and Pillai. 2018). Considering these advantages, GA is a proper tool to train different methods like ANN and ANFIS. It should be noted that the application of classical algorithms such as back propagation in training ANN and ANFIS models to solve complex problems cannot be considered as an efficient tool, because they have problems including high simulation time and misleading in the local optimization. In this paper, GA is utilized to train ANFIS in the simulation of the DC. In the present work, after the determination of the initial values related to GA, the initial population is randomly produced by this algorithm. In addition, the search for finding the best fitness value for modeling the DC is performed through the procedure defined in this methodology. The fitness function (FF) introduced in the current investigation is a root mean square error (RMSE) providing the difference between the predicted and estimated values of the objective function as a number (RMSE). After the random creation of the first population known entitled "initial chromosomes", the chromosomes with the suitable performance in optimizing the fitness function are selected and transferred to the next generation. In this case, if the performance of the chromosomes is in a way that is acceptable in the prediction of the DC, then the completion ends, otherwise a new generation is created and the generation optimization process continues by generating new chromosomes by GA. The optimization cycle in GA is repeated until reaching the optimal answer or the number of iterations defined in the algorithm. Once the optimization by GA ends, the rest of the modeling continues similar to the classical ANFIS. Using the trying and error method, the number of iterations is considered equal to 500 so that more increasing this parameter will not have an important impact on the optimization outcomes. Furthermore, the value of the initial population is considered in the range of 30-300 and 200 is chosen as the optimized amount. Besides, the percent of mutation and crossover for the optimal model are 0.15 and 0.85. The ANFIS-GA flowchart for DC modeling is shown in Fig. 5.

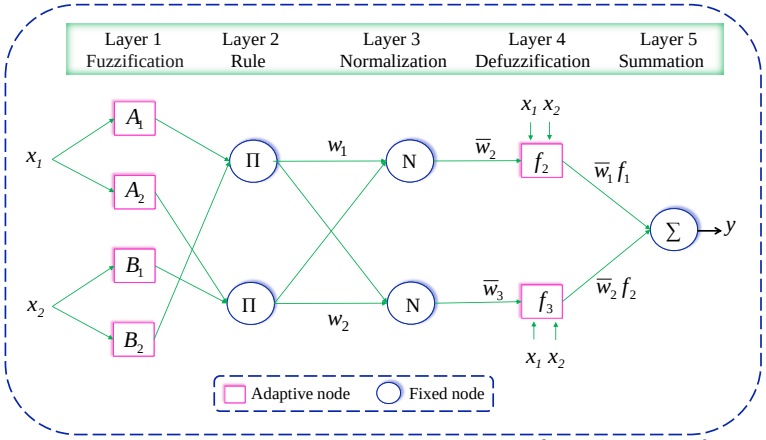

$$O_i^1 = \text{gaussmf}(x,\sigma,c) = \mu_{A_i}(x) = exp\left(-\frac{\|x-c_i\|^2}{2\sigma_i^2}\right)$$

$$O_i^2 = w_i = \mu_{A_i}(x)\cdot\mu_{B_i}(y) \quad i=1,2$$

$$O_i^3 = \overline{w}_i = \frac{w_i}{\sum_{i=1}^{n} w_i} = \frac{w_i}{w_1+w_2+w_3+w_4} \qquad i\in\{1,2,3,4\}$$

$$O_i^4 = \overline{w}_i f_i = \overline{w}_i(p_i x + q_i y + r_i)$$

$$O_i^5 = \sum_{i=1}^{n} \overline{w}_i f_i = \frac{\sum_{i=1}^{n} \overline{w}_i f_i}{\sum_{i=1}^{n} \overline{w}_i}$$

Fig. 4. Structure of ANFIS network.

2.5. Application of Particle Swarm optimization (PSO) for training ANFIS

The PSO method presented for the first time by Kennedy 1995 is an important evolutionary models in solving non-linear complex issues. Some of the most significant benefits of the PSO are: easy implementation, low probability of trapping in local minimum, low

computing volume and high convergence speed. Hence, this algorithm is a reliable tool for training intelligent models, which in recent years has used many uses in various engineering sciences, especially water and hydraulic engineering (Gholami et al. 2018; Qasem et al. 2017; Shaghaghi et al. 2017). In fact, in this algorithm, every particle is aware of the situations experienced by itself and other particles. If we consider the particle i placed in a d-dimensional space of the desired problem, its position is defined by Eq. 3. The parameter t defined in this Eq. shows the iteration related to the desired particle. The particle introduced in this Eq. has velocity so that transfers the desired particle to the next generation. The velocity related to the particle i in the t^{th} particle is presented by Eq. 4. As discussed, each particle is aware of the other particle position, thus each particle should have a memory to recall its position as well as others. This memory is evaluated by Eq. 5.

$$X_i^t = (x_{i1}^t, x_{i2}^t, ..., x_{id}^t) \quad (3)$$

$$V_i^t = (v_{i1}^t, v_{i2}^t, ..., v_{id}^t) \quad (4)$$

$$P_i^t = (p_{i1}^t, p_{i2}^t, ..., p_{id}^t) \quad (5)$$

Based on the position and velocity definitions, different particle positions are updated in each iteration using the best location achieved in the population (gbest) and the best solution (pbest). By identifying these two factors, the speed and location of each objective are adjusted as below:

$$V_i(t+1) = wV_i(t) + C_1 r_{1,i}(t)(p_i(t) - X_i(t)) + C_2 r_{2,i}(t)(p_g(t) - X_i(t)) \quad (6)$$

$$X_i(t+1) = X_i(t) + V_i(t+1) \quad (7)$$

here,*C*1 and *C*2 are learning parameters, r_1 and r_2 are two random parameters in the domain of [0, 1], *t* is the repetition value and w is the inertia weight considered in the range of [0, 1]. Also, according to Ebtehaj and Bonakdari 2016 to consider the values of C1 and C2 more than 2, the value of these two parameters are considered C1 = C2 = 2.65. It is necessary that the variables related to the optimization algorithms are defined so that the model reaches its optimum state. In complex problems such as the present study, classical algorithms such as back propagation may become trapped in the local minimum and result in model overfitting. Therefore, the selection of the parameters related to the optimization algorithm minimizing the fitness function is crucially important. The number of iterations is considered 500, so that more increasing will not change the fitness function value. The initial population is considered in the range of 30-300. In addition, 200 is chosen as the optimal value. Furthermore, the values of the minimum optimal and the maximum inertia weight are tuned as 0.3 and 0.9.
The optimization process in PSO is carried out in such a way that the pbest belonging to all particles is stored in each generation. After that, gbest is found and speed and location of each objective are adjusted using these two factors. This cycle continues until the model converges or the number of considered iterations ends. Different stages of modeling the DC through the ANFIS-PSO approach is presented in Fig. 6.

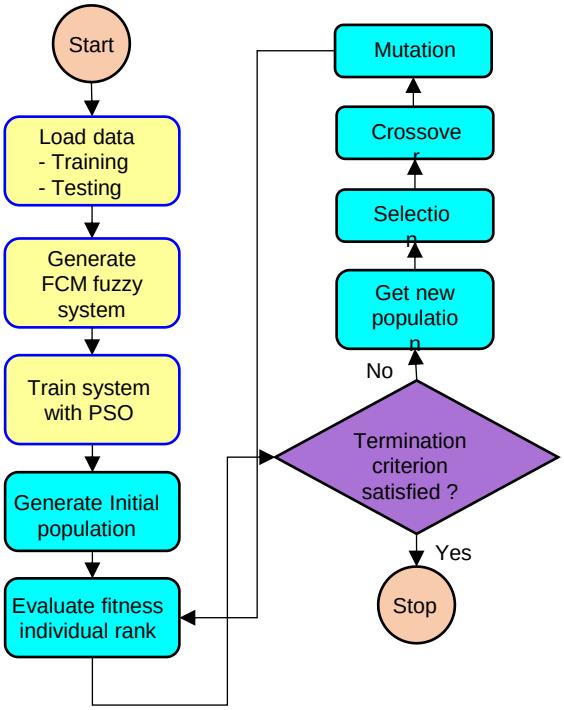

Fig. 5. Flowchart of ANFIS-GA.

2.6. Application of Firefly Algorithm (FFA) for training ANFIS

Similar to GA and PSO, the FFA is an evolutionary method presented by Yang. 2008 regarding the following assumptions:
1) Regardless of their gender, fireflies are attracted by other fireflies 2) the attraction is relative; less bright fireflies are attracted towards brighter fireflies. The firefly moves randomly if there is no brighter one and 3) by light emitting as much as possible, a firefly attract the bait towards itself to share the victim with others. The FFA mimics the firefly's manner in the search for nourishment and social behavior. In nature, fireflies voyage by random and individually one that discovers the most suitable seduction radiates additional glow and entices others.

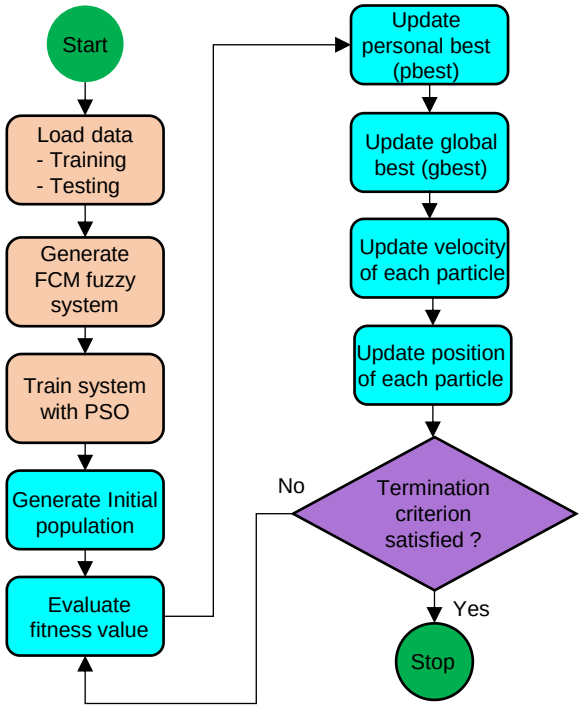

Fig. 6. Flowchart of ANFIS-PSO model.

As the space between two fireflies enhances their ratio of absorption decreases. That is, distance has an inverse relation to speed and attraction. This method owns 2 essential elements:
a) Variations of light strength;

Light strength relies on the cost function magnitude. Hence, in minimalization (maximization) issues, the brighter firefly absorbs

fireflies with lesser brightness. Presume that *n* is the population of fireflies, x_i is the i^{th} term situation and $f(x_i)$ is the cost function. Thus, the brightness of each firefly is the same as the cost function value:

$$I_i \propto f(x_i), 1 \le i \le n \quad (8)$$

b) Moving toward brighter firefly
Single firefly owns a bright characteristic showing how much it is robust. This is a relative amount varying by alteration of the space between firefly i and firefly j. The absorption function is determined as below:

$$\beta(r) = \beta_0 e^{-\gamma r^2} \quad (9)$$

here, β_0 is the absorption degree as a function of r=0 and γ. The displacement of Firefly i with the situation x_i is computed as below:

$$x_i(t+1) = x_i(t) + \beta_r(x_i - x_j) \quad (10)$$

To form ANFIS through the FA, first, the problem environment or domain of variables that ought to be optimized, and the ability assessment function may be created.. In the current work, RMSE is applied as the FF for assessment of the efficiency of the ANFIS network trained by the FFA. Single firefly comprises several subsequent and antecedent variables. To initial the modeling, the first population of FF is defined by random. Each of the fireflies may use the ANFIS variables. With regard to the brightness magnitude for each firefly, the abortion is calculated and juxtaposed with others and less bright FF displacement toward lighter ones. Subsequently, the fitness function amount is computed. The procedure repeated till reaching the defined repetition or the minimum amount of the favorable FF. The algorithm flowchart presented in this study is provided in Fig. 7.

2.7. Computational Fluid Dynamics (CFD) model
2.7.1. Governing Eqs.

At this work, for unsteady flow simulation and incompressible water, the continuity and averaged Naiver-Stocks Eqs. are applied as below:

$$\frac{\partial U_i}{\partial X_i} = 0.0 \quad (11)$$

$$\frac{\partial U_i}{\partial t} + U_j \frac{\partial U_i}{\partial X_j} = \frac{1}{\rho}\frac{\partial}{\partial X_j}\left[-P\delta_{ij} + \rho \nu_t\left(\frac{\partial U_i}{\partial X_j} + \frac{\partial U_j}{\partial X_i}\right)\right] \quad (12)$$

where, U_i ,U_j and X $(i, j = 1,2,3)$ are the speed components and axes in the Cartesian coordinate. Furthermore, *t*,*ρ*, *p*, δ_{ij}, (*i*,*j* = 1,2,3), and ν_t are time, fluid viscosity, pressure, Kronecker delta and turbulent eddy-viscosity, individually. Eqs. 11 and 12 are used by the FLOW3D model to solve the flow field parameters comprising the velocity, pressure, etc. Initially, the flow field is in the unsteady circumstance; however, it became steady after solving the problem at the end of the simulation process.

In modeling the flow field, the estimation of the free surface is significantly vital which is one of the most significant approaches to estimate the free surface. The volumetric part of water by the variable *F*. In this method, if a specific cell is full of water, *F* = 1, otherwise, If this cell is empty, *F* = 0 and 0<*F*<1 shows that the stated the cell possesses both air and water fluids. In the present work, the VOF approach is performed to forecast the changes of the water surface. The FLOW-3D software was utilized for the simulation of the CFD part. The geometry of the structure was produced in the FLOW-3D environment. The applied geometry was a three-dimensional model.

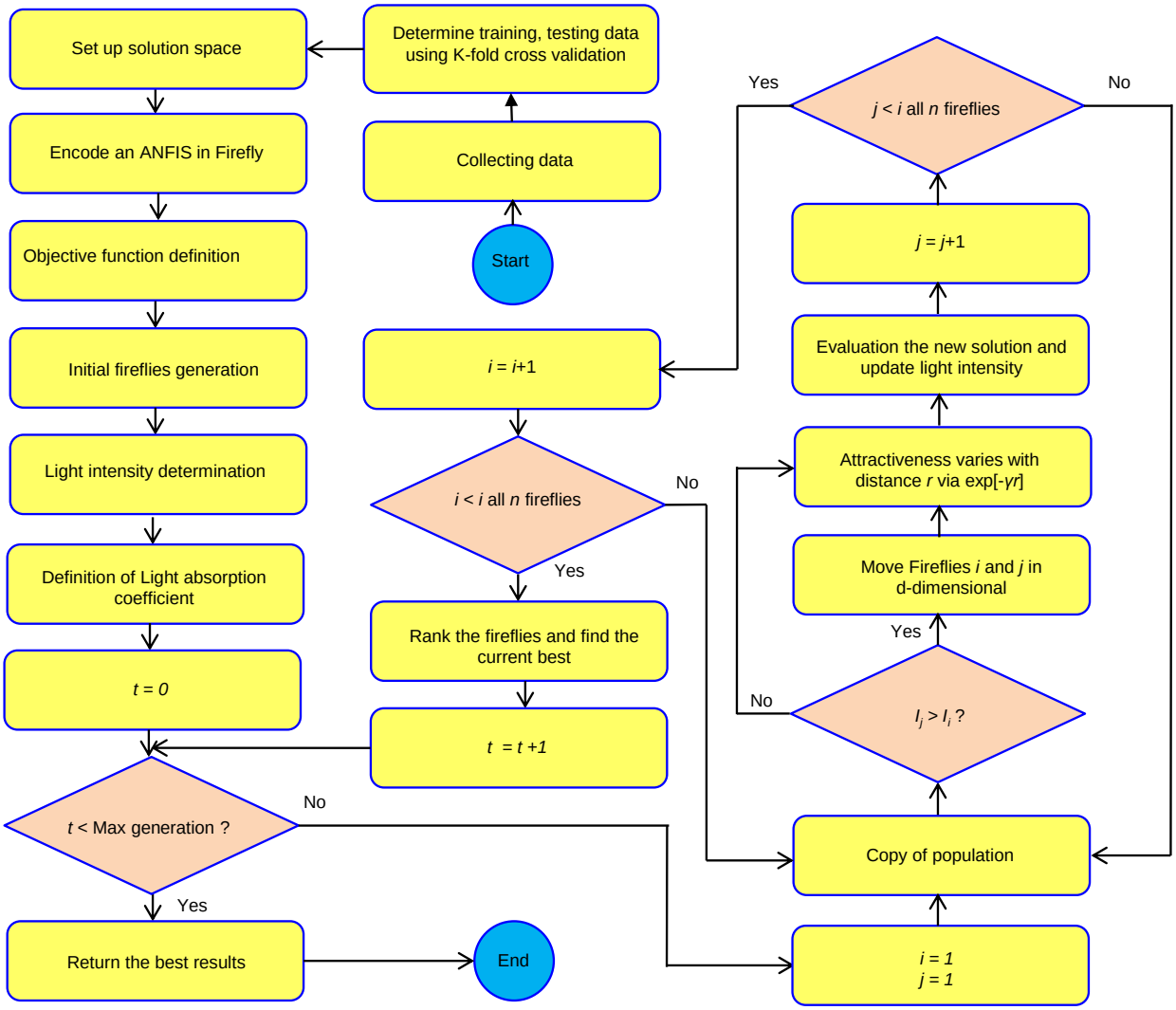

Fig. 7. Flowchart of ANFIS-FFA model.

2.7.2. Boundary condition (BC)

In this paper, for validation of the CFD outcomes, the laboratory values measured by Bagheri et al. 2014 are performed. Hence, the boundary conditions selected for the CFD method ought to be coordinated with laboratory results. Thus, thanks to the certainty of the discharge and the flow depth at the main inlet, values of discharge and certain flow depths which regarded as the “Volume Flow Rate” BC are employed. Moreover, the "Outflow" BC is considered at the main outlet. Sidewalls and bottom of the simulation are assumed as the "Wall" BC. Furthermore, the upper layer of the flow field is regarded as the "Symmetry" BC.

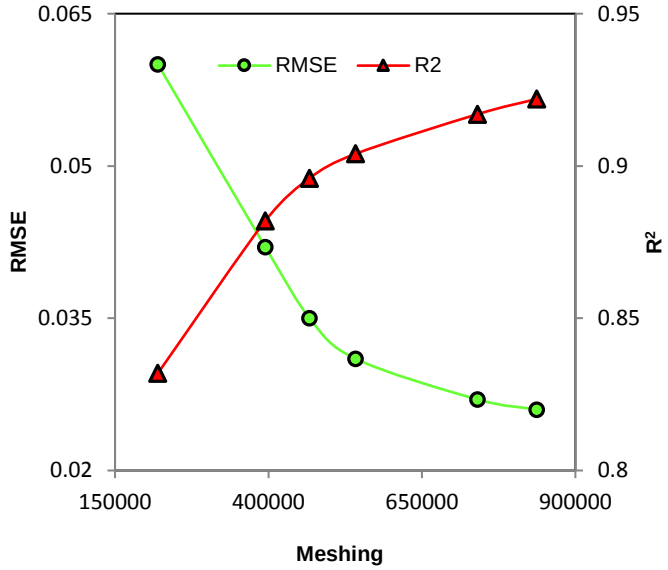

Fig. 8. Changes of RMSE and R^2 versus the number of flow field computational elements for simulating discharge coefficient.

2.7.3. Performance assessment indices

In this paper, to assess the CFD model performance, the determination coefficient (R^2), root mean square error (RMSE), mean absolute percent error (MAPE), and scatter index (SI) are used as below:

$$MAPE = 100 \times \frac{1}{n}\sum_{i=1}^{n}\left(\frac{\left|R_{(\mathrm{Predicted})_i} - R_{(Observed)_i}\right|}{R_{(\mathrm{Predicted})_i}}\right) \quad (14)$$

$$RMSE = \sqrt{\frac{1}{n}\sum_{i=1}^{n}\left(R_{(\mathrm{Predicted})_i} - R_{(Observed)_i}\right)^2} \quad (15)$$

$$R^2 = \frac{\left(n\sum_{i=1}^{n} R_{(\mathrm{Predicted})i} R_{(Observed)i} - \sum_{i=1}^{n} R_{(\mathrm{Predicted})i}\sum_{i=1}^{n} R_{(Observed)i}\right)^2}{\left(n\sum_{i=1}^{n}\left(R_{(\mathrm{Predicted})i}\right)^2 - \sum_{i=1}^{n}\left(R_{(\mathrm{Predicted})i}\right)^2\right)\left(n\sum_{i=1}^{n}\left(R_{(Observed)i}\right)^2 - \sum_{i=1}^{n}\left(R_{(Observed)i}\right)^2\right)} \quad (16)$$

$$SI = \frac{RMSE}{\overline{(R)}_{(Observed)i}} \quad (17)$$

here, the amount of $(R)_{(oberved)\ i}$, $(R)_{(predicted)\ i}$, $(\bar{R})_{(oberved)\ i}$, and n are laboratory amount, outcomes predicted by CFD simulation, the average of laboratory model, and the number of laboratory measurements. It must be stated that five models are produced for identifying the most influential inputs.

2.7.4. Meshing

The computational flow field is gridded by six gridding types. First, the number of computational elements (NCE) is considered 220000. Then, the value of error is approximated by enhancing the NCE. The changes of RMSE and R^2 values versus enhancing the NCE for simulating the discharge coefficient are illustrated in Fig. 8. As shown, by increasing the flow field elements the error value decreases. Finally, the flow field is separated by 740600 computational cells. For instance, the RMSE and R^2 indices for 220000 elements are surmised as 0.060 and 0.832. In contrast, RMSE and R^2 for 740600 computational cells are obtained 0.027 and 0.917, respectively. The meshed geometry applied is demonstrated in Fig. 9.

3. Results and discussion

3.1. ANFIS

The accuracy of the ANFIS method is examined. To identify the most influential input, five ANFIS models are created via the combination of the inputs. Then, by eliminating each of these parameters, the best model along with the effective parameter are determined. In Fig. 10, the criteria are shown for the artificial intelligence models. For example, ANFIS1 estimates DC by utilizing all inputs. Such model calculated the R^2 and SI criteria as 0.893 and 0.065. In addition, the (RMSE) and (MAPE) indices for this model are also obtained 0.032 and 4.893. Also, four models are developed by combining three input parameters (ANFIS 2 to ANFIS 5). To estimate the DC by ANFIS 2, the impact of P/y_1 is eliminated. In other words, that model forecasted the DC by Fr, b/B, b/y_1. The R^2, SI, and RMSE amount for this model are computed 0.800, 0.089 and 0.043, individually. Moreover, MAPE for ANFIS 2 is equal to 6.186. For modeling the DC by ANFIS 3, the impact of the $b/y_1$is neglected. This model approximated the objective function by Fr, b/B, P/y_1. Regarding the simulation outcomes, ANFIS 3 possesses the highest precision amongst the models with three input parameters. For ANFIS 4, the impact of the b/B is removed and such model estimated the DC utilizing Fr, b/y_1, P/y_1. Among all ANFIS models, this model has the highest level of error. The RMSE and MAPE criteria for ANFIS 4 are calculated as 0.049 and 7.835. In addition, the values of the SI and R^2 are 0.101 and 0.742. However, ANFIS 5 estimates the DC values by b/B, b/y_1, P/y_1. For that model, the flow Froude number influence is neglected.Based on the results obtained from the simulation outcomes, ANFIS 1 is regarded as the premium model. Furthermore, the b/B parameter is recognized as the most significant input.

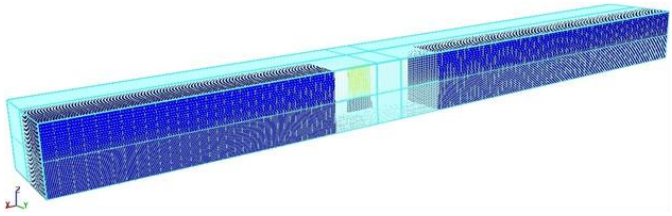

Fig. 9. The meshed geometry applied in this study.

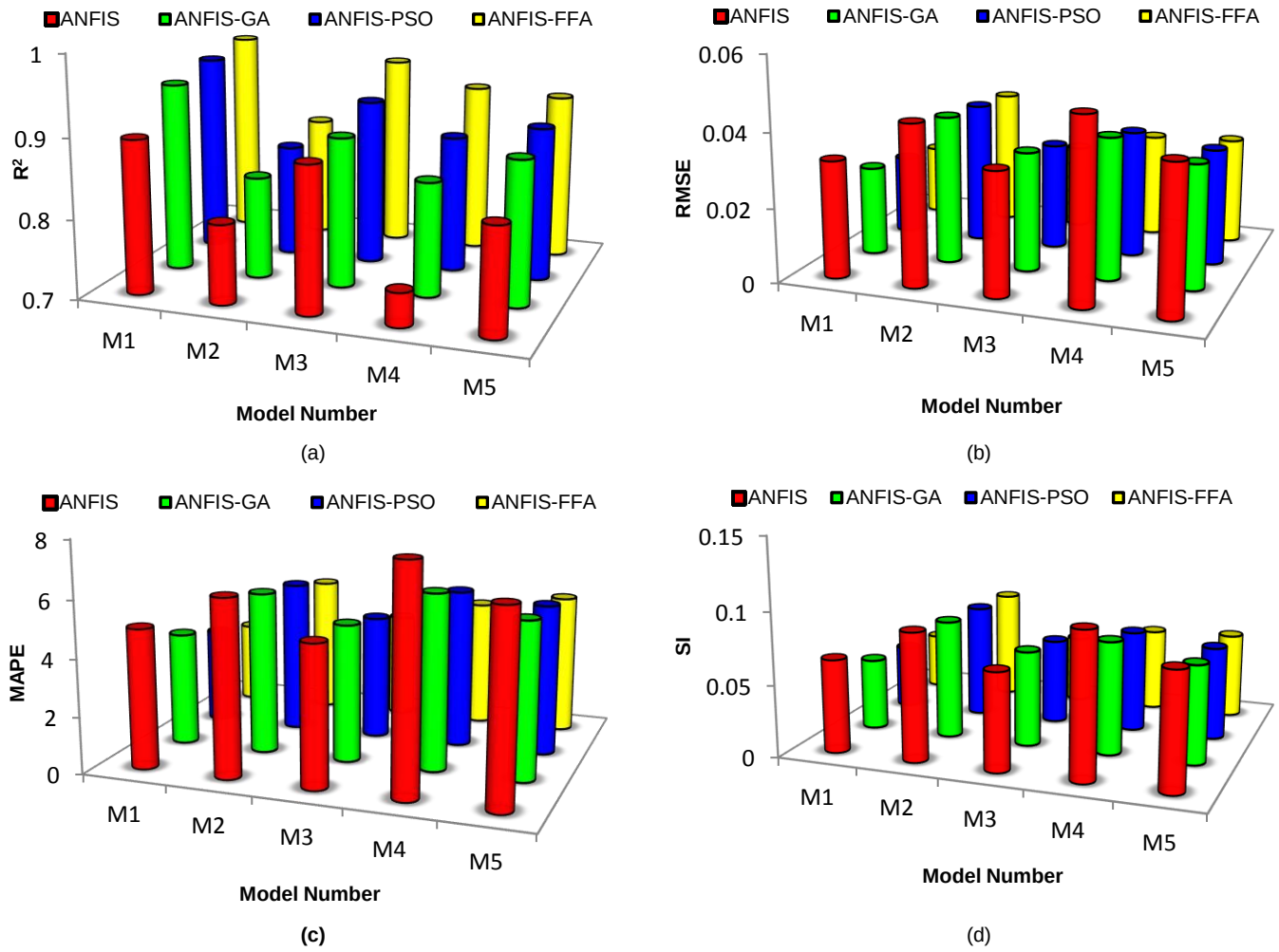

Fig. 10. Comparison of all statistical indices for different artificial intelligence models (a) R^2 (b) RMSE (c) MAPE (d) SI

3.2. Optimization of ANFIS

Below, the ANFIS network is optimized. To this end, one of the most important optimization algorithms such as GA, PSO and FFA is utilized. In general, the aim is finding the most optimal possible answer through the combination of these algorithms and the ANFIS network.

3.2.1. ANFIS-GA

In the upcoming parts, the ANFIS-GA models are evaluated. In Fig. 11 to 15, the criteria of various ANFIS-GA models are juxtaposed with each other. Based on the modeling outcomes, ANFIS-GA1 owns the highest precision amongst these models. It possesses a good correlation with the laboratory data. R^2 is approximated 0.938. Besides, MAPE and RMSE for ANFIS-GA1 are surmised at 3.964 and 0.024. In addition, in the models with 3 inputs, ANFIS-GA2 owns the lowest precision. Values of MAPE, R^2 and SI are computed 5.676, 0.828 and 0.082. In comparison with other methods, it possesses a low relation with the observational data. For ANFIS-GA3, the RMSE and MAPE indices are computed 0.032 and 4.829. Hence, amongst the models with three inputs, ANFIS-GA3 owns the best performance. For the model, R^2 and SI are computed equal to 0.888 and 0.066. In ANFIS-GA4, the RMSE, MAPE, and SI are at 0.038, 6.157 and 0.078, in turn. For ANFIS-GA5, the R^2 and SI criteria are individually obtained 0.881 and 0.068. Thus, ANFIS-GA1 estimates the DC with reasonable efficiency. Indeed, the ANFIS-GA models sensitivity analysis demonstrates that the P/y_1 input is the most important input.

3.2.2. ANFIS-PSO

The outcomes of the ANFIS-PSO method are evaluated. For the ANFIS-PSO1, the R^2 and SI indices are at 0.951 and 0.044. In addition, MAPE and RMSE for such model are recognized as 3.349 and 0.021. However, R^2 and RMSE for ANFIS-PSO2 are 0.842 and 0.038, respectively. Furthermore, MAPE is estimated 5.359 for this model. The ANFIS-PSO3 hybrid model calculates the SI, MAPE, and R^2 to be 372.059, 0.4 and 0.91. Moreover, for the ANFIS-PSO4 model, R^2 and Si are computed 0.872 and 0.071, in turn. The MAPE and R^2 criteria for the ANFIS-PSO5 model are, individually, 5.307 and 0.893. The SI and RMSE amounts for this model are 0.065 and 0.032, in turn. Based on the results of the ANFIS-PSO method, ANFIS-PSO1 possesses the highest level of correlation with the observed values. The sensitivity analysis of the ANFIS-PSO models exhibits that the P/y_1 input is detected as the most effective input parameter.

3.2.3. ANFIS-FFA

The accuracy of the ANFIS-FFA methodology are studied. ANFIS-FFA1 predicts the DC values utilizing all inputs. For this mode, the RMSE and SI are, in turn, 0.019 and 0.039. Moreover, R^2 is approximated 0.961 for this model. As discussed above, in the present investigation, the impact of the inputs are eliminated for identifying the most significant input on the DC and the ANFIS-FFA2 to ANFIS-FFA5 methods are produced. As an example, for ANFIS-FFA2, the MAPE, RMSE, and SI criteria are calculated 4.834, 0.037, and 0.076, individually. Furthermore, R^2 is estimated equal to 0.853 for this model. In the models with three inputs, ANFIS-FFA2 owns the biggest error. For ANFIS-FFA3, R^2 and SI are obtained 0.943 and 0.047, in turn. Moreover, the RMSE and MAPE values are approximated to be 0.23 and 3.719. For the ANFIS-FFA4 model, the MAPE and RMSE are, respectively, 4.457 and 0.028. In the following, ANFIS-FFA5 is evaluated. For example, the RMSE and SI statistical indices are obtained, individually, as 0.029 and 0.059. So, ANFIS-FFA1 possesses the highest level of correlation with the observed measurements among the ANFIS-FFA methods. The sensitivity analysis of the ANFIS-FFA methods demonstrates that the P/y_1 input is identified as the most remarkable input. The scatter plots of these ML methods are illustrated in Figs. 11 to 15.

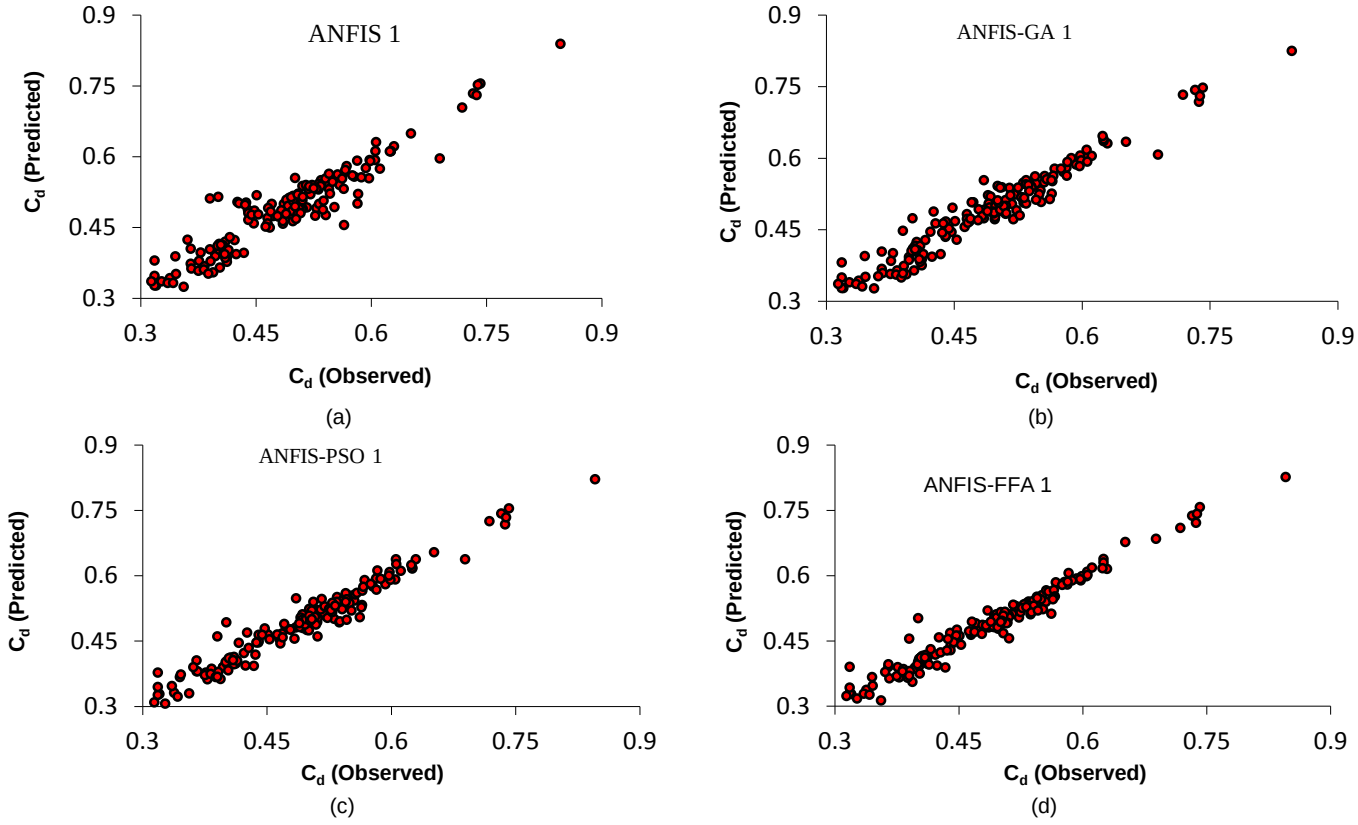

Fig. 11. Scatter plots for ML method 1 (a) ANFIS 1 (b) ANFIS-GA 1 (c) ANFIS-PSO 1 (d) ANFIS-FFA 1

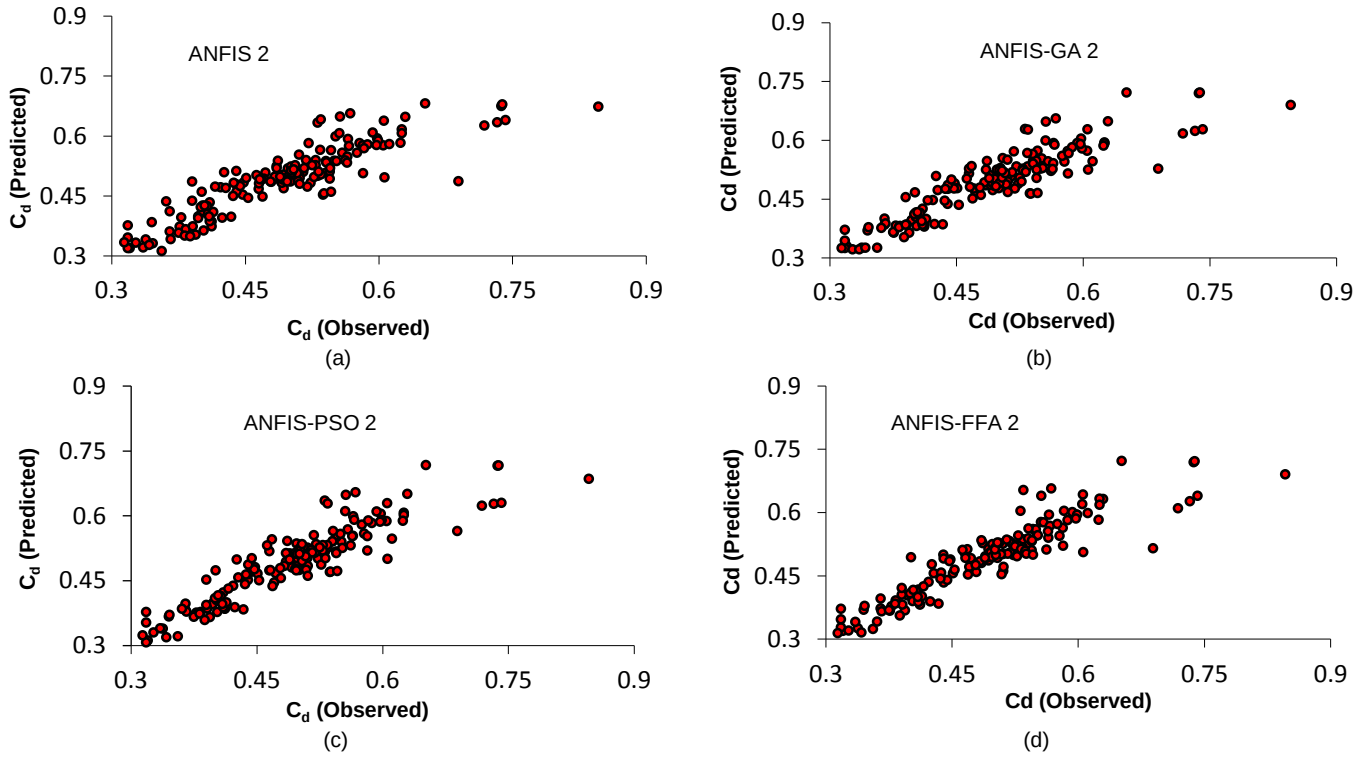

Fig.12. Scatter plots for ML method 2 (a) ANFIS 2 (b) ANFIS-GA 2 (c) ANFIS-PSO 2 (d) ANFIS-FFA 2.

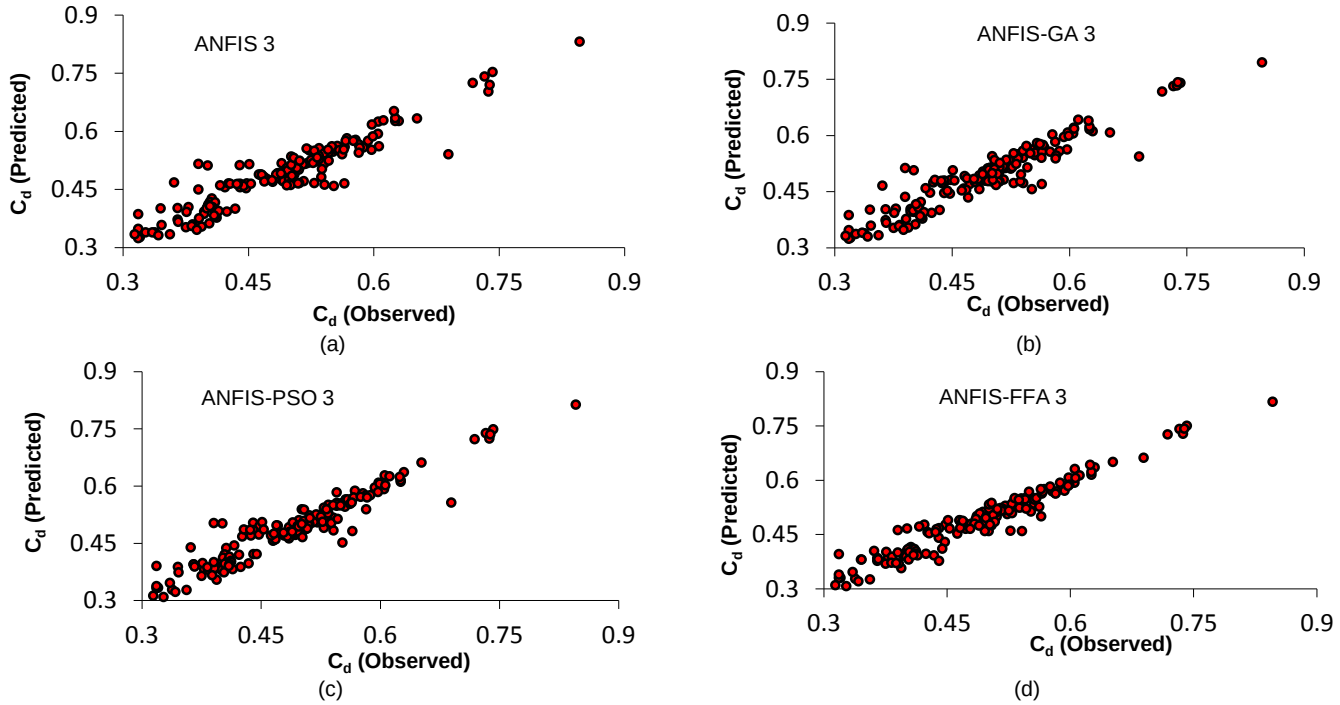

Fig.13. Scatter plots for ML method 3 (a) ANFIS 3 (b) ANFIS-GA 3 (c) ANFIS-PSO 3 (d) ANFIS-FFA 3.

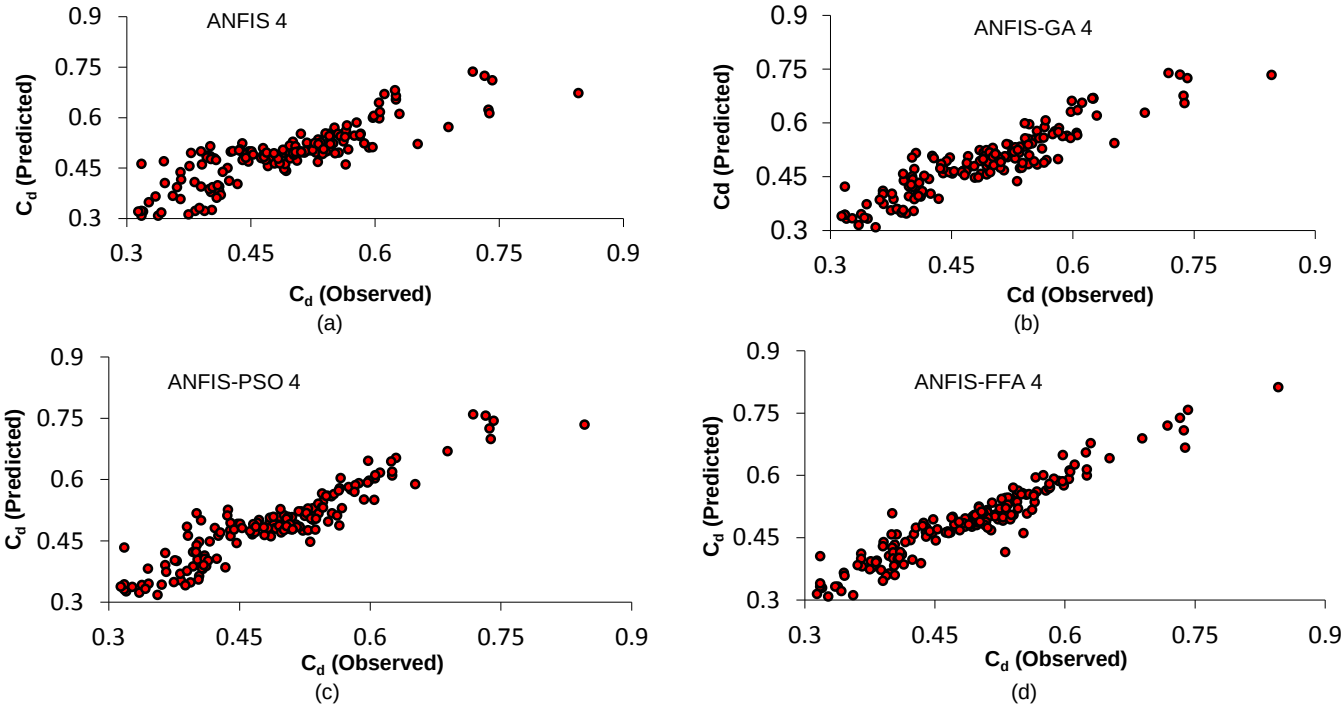

Fig.14. Scatter plots for ML method 4 (a) ANFIS 4 (b) ANFIS-GA 4 (c) ANFIS-PSO 4 (d) ANFIS-FFA 4.

The ML methods are investigated in more details. In order to further study the precision of the ML methods, the discrepancy ratio (DR) of the mentioned methods are assessed. The variable is the simulated DC to the laboratory value ratio:

$$DR = R_{Predicted} / R_{Observed} \quad (18)$$

The closeness of the parameter to one exhibits the closeness of predicted values to experimental ones. In addition, DR_{max}, DR_{min} and DR_{ave} are also calculated for the ANFIS1, ANFIS-GA1, ANFIS-PSO1 and ANFIS-FFA1 models. Furthermore, the changes of DR versus the observed DC are plotted in Fig. 16. For example, the DR_{ave} value for the ANFIS1 model is surmised as 1.005. In that model, the values of DR_{max} and DR_{min} are calculated, respectively, 1.310 and 0.805. Also, the DR_{ave} value for the ANFIS-GA1 and ANFIS-PSO1 models are approximated as 1.003 and 1.0023, respectively. The DR_{ave} value for the ANFIS-FFA1 model is equal to 1.0021. Thus, the closest amount of DR_{ave} to 1 is obtained for ANFIS-FFA1.

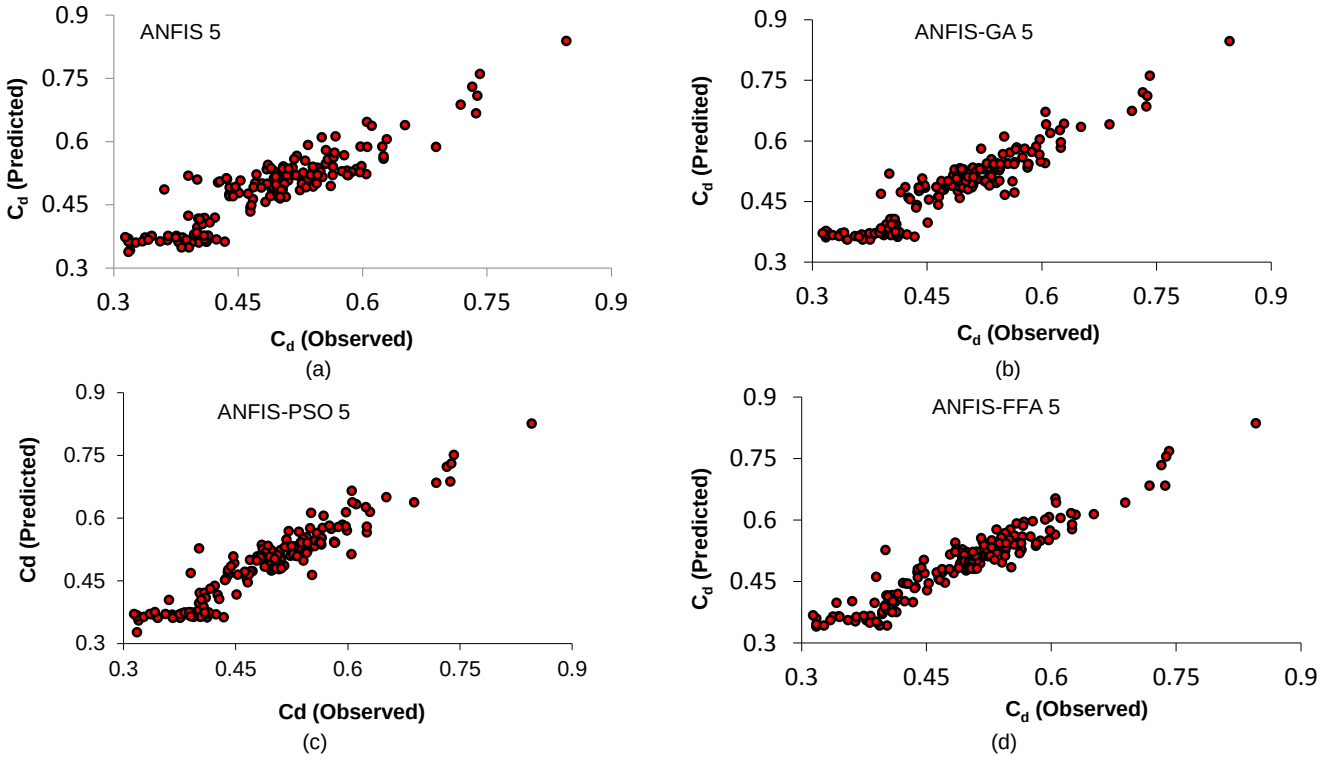

Fig. 15. Scatter plots for ML method 5 (a) ANFIS 5 (b) ANFIS-GA 5 (c) ANFIS-PSO 5 (d) ANFIS-FFA 5.

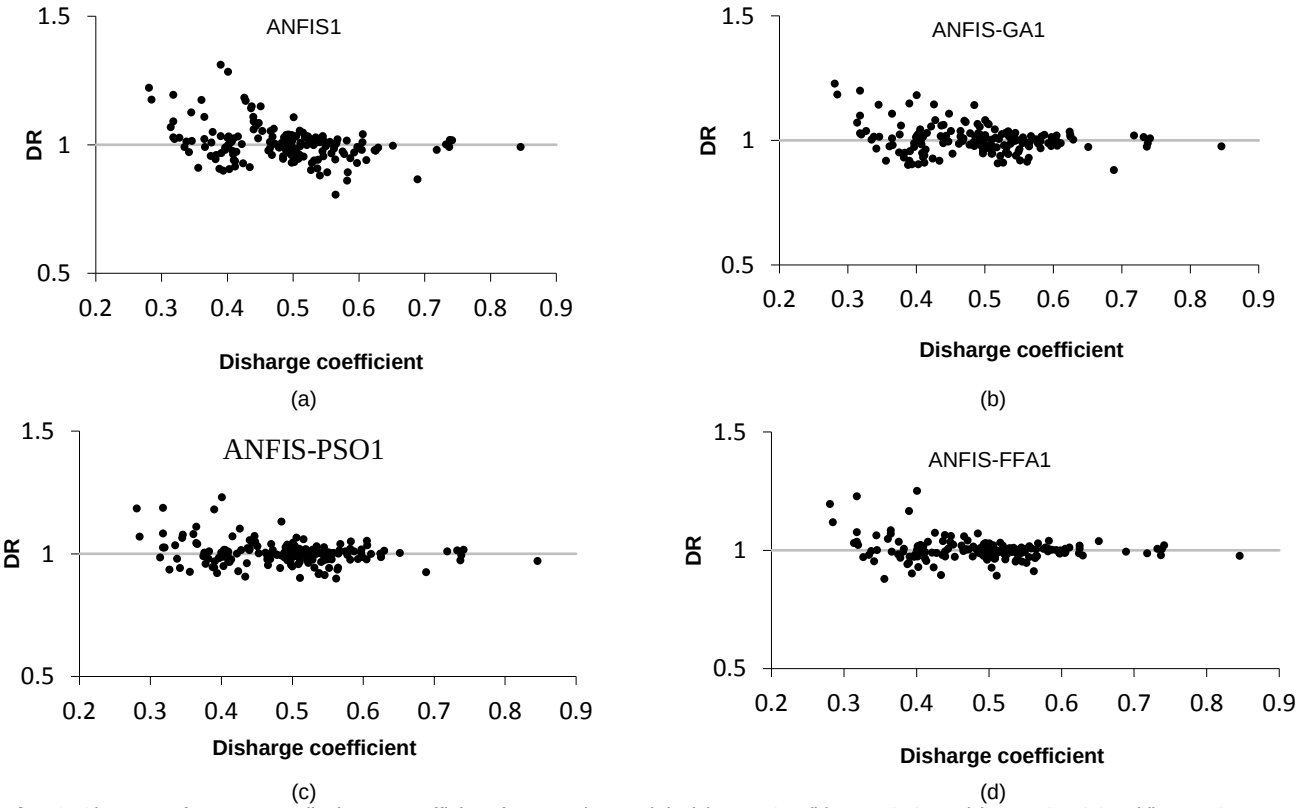

Fig.16. Changes of DR versus discharge coefficient for superior models (a) ANFIS 1 (b) ANFIS-GA 1 (c) ANFIS-PSO 1 (d) ANFIS-FFA 1

3.3. CFD results

The outcomes of the DC simulation done by the CFD method are studied. The scatter plots of the simulated and observed discharge coefficients are drawn in Fig. 17. According to the modeling outcomes, the R^2 and RMSE criteria for the DC approximated by the CFD model are surmised as 0.917 and 0.027, in turn; while, the SI and MAPE statistical indices for this method are at 0.044 and 4.107, individually. As can be seen, the CFD method simulates the DC with good performance.

3.4. Superior models

3.4.1. Relative error

Relative error outcomes for the ANFIS1, ANFIS-GA1, ANFIS-PSO1, ANFIS-FFA1 and CFD methods are performed (see Fig. 18). Regarding the analysis, approximately 67% of the outcomes modeled by ANFIS 1 show an inaccuracy smaller than 5%, while roughly 71% of the DC modeled by the ANFIS-GA1 method own an error of smaller than 5%. Moreover, the error analysis show that near 18% of the DC estimated by ANFIS-PSO1 possess an inaccuracy between 5% and 10%. The analysis reveals that about 5% of the ANFIS-FFA1 outcomes

own an error of greater than 10%. However, almost 28% of the DC simulated by demonstrate an inaccuracy between 5% and 10%. The error analysis proves that the ANFIS-FFA1 hybrid method is further precise than the other models. The inputs b/B and Ply_1 are the most significant variables.

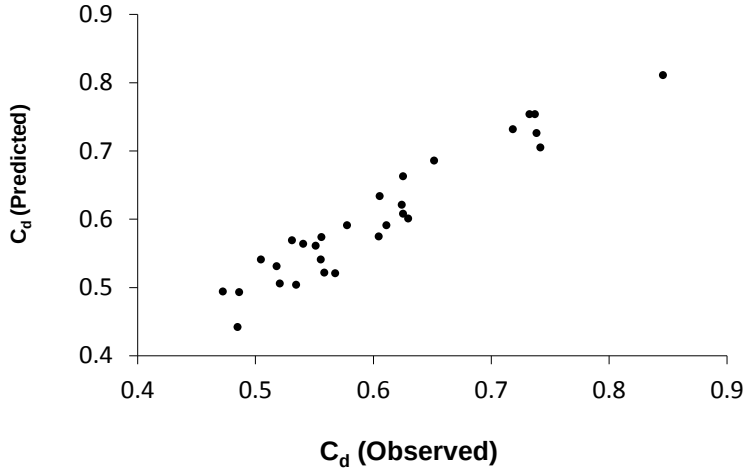

Fig. 17. DC predicted by CFD and comparison with observed values.

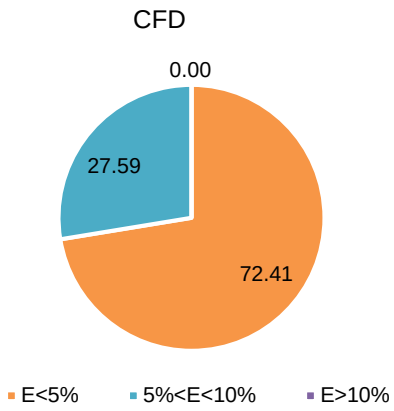

(e)

Fig. 18. Relative error distribution for (a) ANFIS1 (b) ANFIS-GA1 (c) ANFIS-PSO1 (d) ANFIS-FFA1 (e) CFD.

3.4.2. Uncertainty analysis (UA)

The UA of the ANFIS 1, ANFIS-GA1, ANFIS-PSO1, ANFIS-FFA1 and CFD methods is conducted. The predicted error by the models (e_j) is approximated as the difference between DC predicted (P_j) and observed ones (e_j = P_j- T_j). The mean value of this inaccuracy is surmised as $\bar{e} = \sum_{j=1}^{n} e_j$, but the standard deviation value of predicted error is computed as $S_e = \sqrt{\sum_{j=1}^{n}(e_j - \bar{e})^2/n - 1}$. The negative value of $\bar{e}$ signifies that the ML model underestimates the DC, whilst the positive value demonstrates that the ML method overestimates the DC. Utilizing the $\bar{e}$ and S_e amounts, a confidence bound (CB) is built around the DC predicted of an error by the Wilson score method, without the continuity correction. Besides, by ±1.96S_e causes the formation of a 95% CB roughly which is denoted by 95% PEI (Azimi et al. 2018b). The parameters of the uncertainty analysis of numerical models are listed in Table 2. In such table, "width of uncertainty band" is illustrated by WUB. Regarding the UN, the ANFIS 1, ANFIS-PSO1 and CFD models have an overestimated performance, while ANFIS-GA1 and ANFIS-FFA1 own an underestimated performance. The S_e and $\bar{e}$ values for the CFD method are surmised as 0.011 and -0.003. The WUB for ANFIS-FFA1 is calculated at -0.003. In addition, 95% PEI for the CFD model is obtained between -0.009 and 0.012. For this model, width of uncertainty band is computed -0.011.

The SA is implemented for the best method. The SA is an applicable approach for showing the impact of inputs on the estimation of the DC. Influences of the parameters Fr,b/B,b/y_1, P/y_1 on C_d are evaluated. For example, by assuming other parameters as constant, one parameter changes in the range of $\pm 10\%$ and the outcomes of the superior method for simulating the discharge coefficient are examined and the values of different statistical indices are computed. sensitivity analysis results of all inputs for the superior model are illustrated in Fig. 19 to 22. For instance, the SA of Fr illustrates that the maximum value of R^2 is calculated for 1.01Fr. By contrast, the minimum R^2 and the maximum RMSE, MAPE, and SI are approximated for 0.88Fr. In addition, the maximum error value for the sensitivity analysis of the parameter b/B is calculated when 0.9 of this value is taken into account. Furthermore, the sensitivity analysis of the dimensionless parameter b/y_1 indicates that the highest correlation as well as the lowest error is achieved when b/y_1 is equal to 1. The SA of P/y_1 indicates that the minimum value of R^2 is obtained for 1.1 P/y_1.

Table 2. Uncertainty parameters for numerical methods.

Model	$\bar{e}$	S_e	WUB	95% PEI
ANFIS 1	4.183E-09	0.032	-0.005	-0.005 to 0.005
ANFIS-GA 1	-1.100E-08	0.024	-0.004	-0.004 to 0.004
ANFIS-PSO 1	1.930E-08	0.022	-0.003	-0.003 to 0.003
ANFIS-FFA 1	-5.405E-09	0.019	-0.003	-0.003 to 0.003
CFD	0.001	0.027	-0.011	-0.009 to 0.012

3.5. Sensitivity analysis (SA) for the superior model

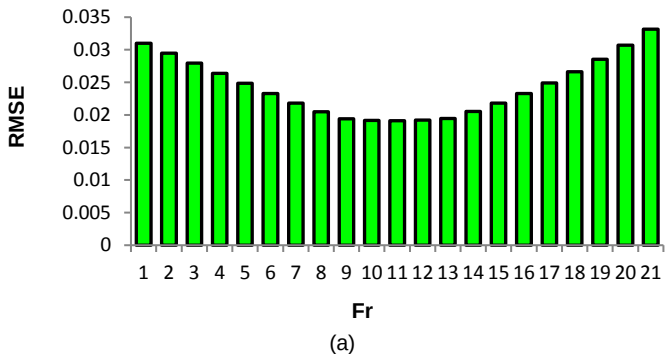

(a)

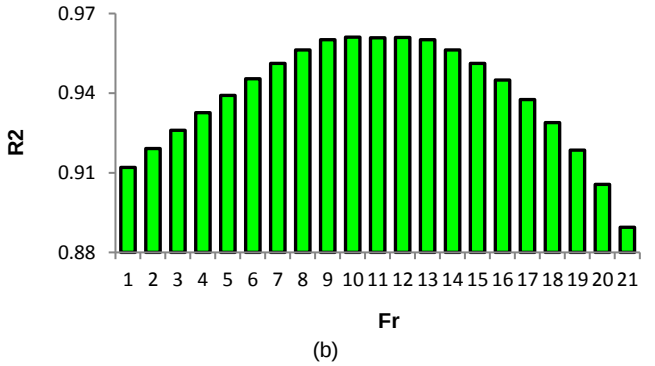

(b)

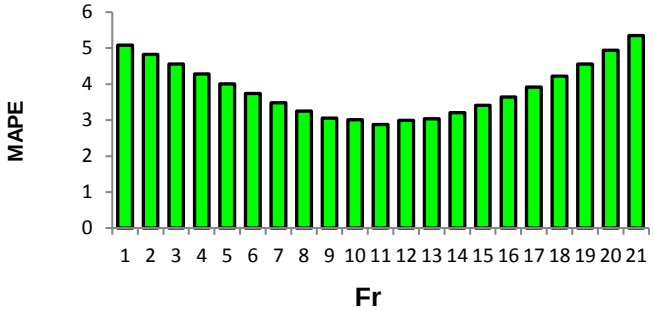

(c)

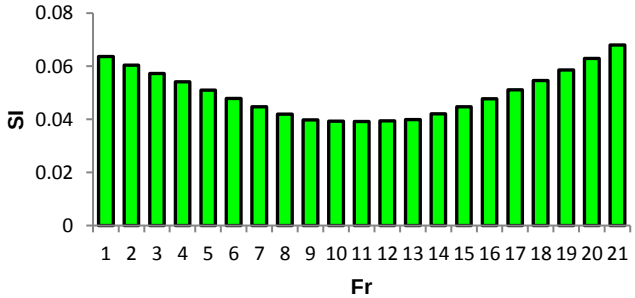

(d)

Fig. 19. Sensitivity analysis for Fr (a) RMSE (b) R^2 (c) MAPE (d) SI.

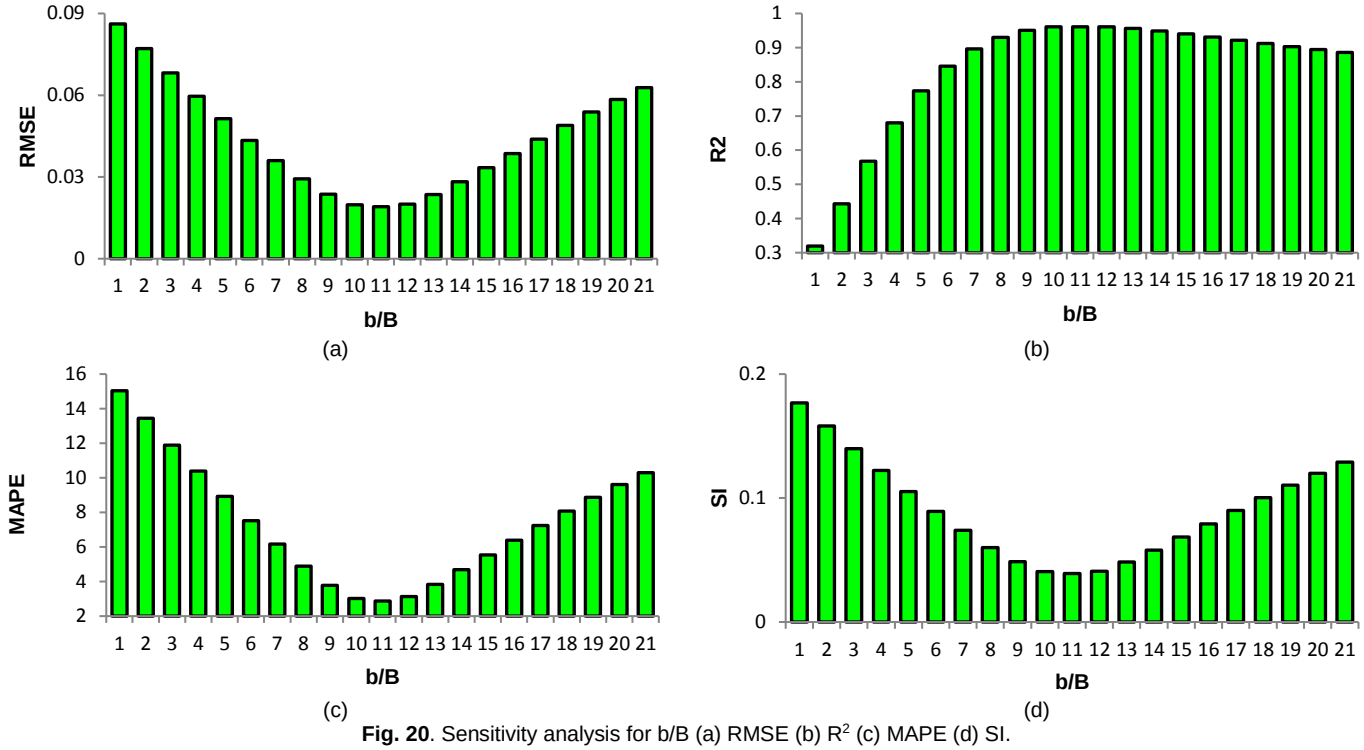

Fig. 20. Sensitivity analysis for b/B (a) RMSE (b) R^2 (c) MAPE (d) SI.

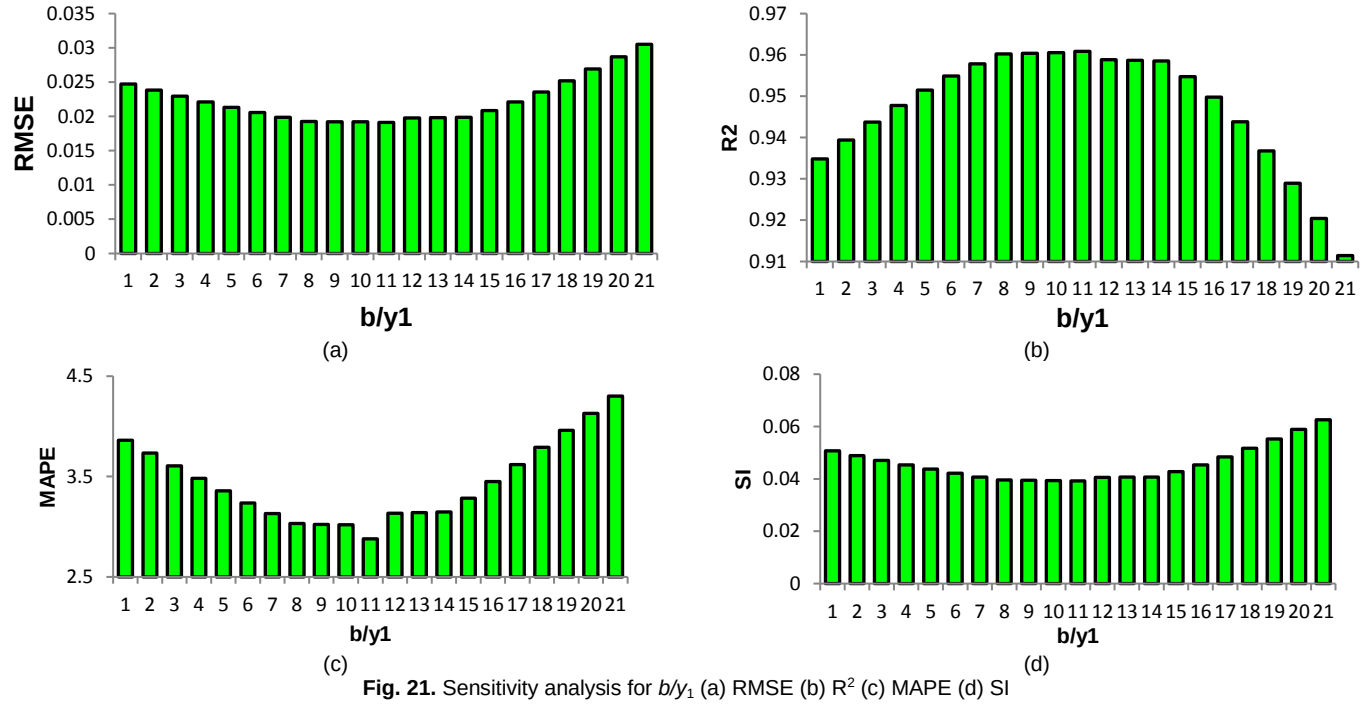

Fig. 21. Sensitivity analysis for b/y_1 (a) RMSE (b) R^2 (c) MAPE (d) SI

The efficiency of the best ANFIS-FFA mode is juxtaposed with three models including Azimi et al.2017, Bagheri et al.2014 and Emiroglu et al 2011 In Table 3, the criteria approximated for such investigations are arranged. As seen, the ANFIS-FFA model has better efficiency in terms of correlation and accuracy to model the discharge coefficient.

Table 3. The statistical indices computed for investigations.

Model	R^2	RMSE	MAPE	SI
ANFIS-FFA	0.9608	0.0191	2.8793	0.039
Emiroglu et al. 2011	0.62	0.137	20.722	0.277
Bagheri et al. 2014	0.265	0.123	20.78	0.234
Azimi et al. 2017	0.816	0.0914	15.31	0.165

The three-dimensional changes of the free flow surface inside the major conduit with side weir are shown in Fig. 23. As seen, when the flow reaches the side overflow, the excess flow passes over the side overflow and is directed into the side tank connected to the side overflow. Due to the fact that the flow conditions inside the main channel are sub-critical, the water depth grows as the flow progresses downstream of the weir. In fact, the flow rate within the major conduit at the beginning of the weir is higher than the flow rate inside the main channel located at the end of the side weir,and regarding the principle of continuity of flow, water depth over weir increases.

3.6. Flow field characteristics

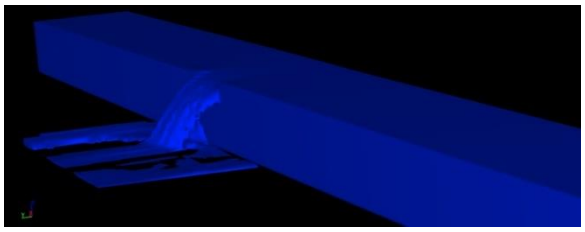

Fig. 23. Three-dimensional variations of the free flow surface in the main channel along side weir.

Pattern of changes of the longitudinal component of flow velocity along the side weir for beginning, middle of opening and the end of the weir is shown in Fig. 24. Regarding this Fig. in each cross-section, by moving from the side of the outer wall to the lateral overflow position, the value of the longitudinal component of the flow velocity increases. In simpler terms, in each cross-section, the maximum longitudinal velocity is predicted near the crest of the lateral overflow. On the other hand, according to the pattern of sub-critical flows along the lateral weir, the longitudinal velocity decreases as the flow moves towards the end of lateral weir.

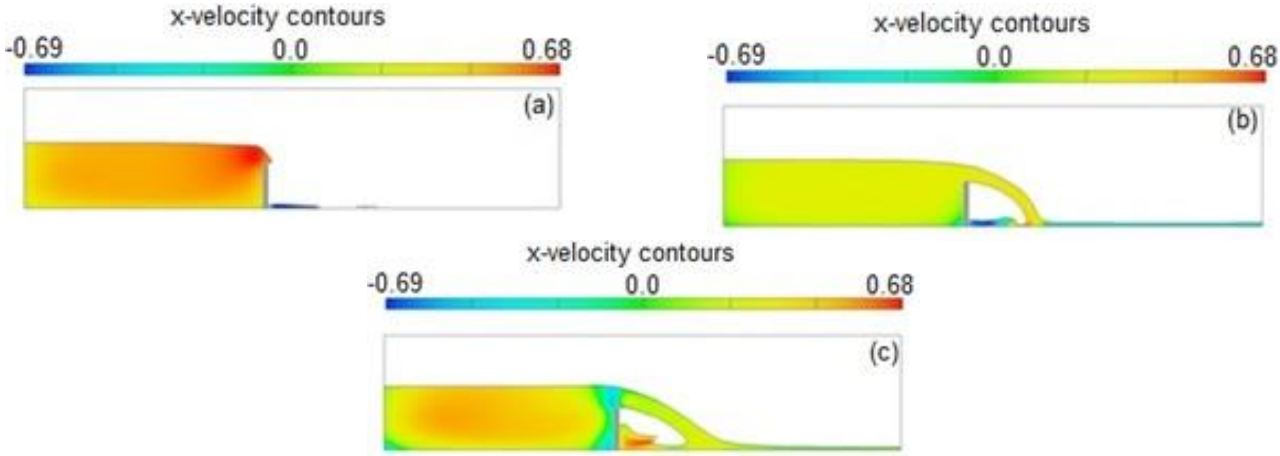

Fig. 24. Pattern of changes in the longitudinal velocity of flow along the side weir (a) beginning of weir (b) middle of weir (c) end of weir.

In the following, the two-dimensional changes of the flow velocity vectors inside the main channel and on the side weir crest are investigated. For this purpose, the changes of the mentioned vectors are shown in Fig. 25. As can be seen, the magnitude of the velocity vectors increased with the approach to the side weir.

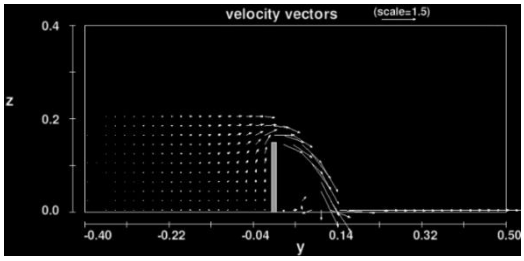

Fig. 25. Two-dimensional variations of flow velocity vectors for side weirs.

4. Conclusions

In this paper, we implemented GA, PSO, and FFA to optimize the ANFIS system for simulating the DC. In other words, five distinct models were introduced for each of the ANFIS, ANFIS-GA, ANFIS-PSO and ANFIS-FFA methods. The analysis of the outcomes identified the best model along with the most significant inputs. After that, the DC was simulated by a CFD method.

- The results indicated that the ANFIS-FFA optimized model estimated the DC with significant higher precision.
- The RMSE, MAPE, and SI criteria for this method were as 0.019, 2.879 and 0.039.
- About 5% of the DC estimated by this model had an error more than 10%.
- By implementing an UA, the CFD method overestimated the DC and the superior ANFIS-FFA model underestimated the DC value.
- SA demonstrated that the impact of all inputs on the estimation of the DC was evaluated in a $\pm 10\%$ range.
- Finally, a MATLAB code was proposed for computing the DC in practice by engineers.

As the most important limitation of this study, the side weirs DC cannot be predicted explicitly using an Eq. by the ANFIS-FFA model. For overcoming this challenge, other machine learning algorithms can be applied to present the explicit Eq.s.

Appendix

The MATLAB code for estimating DC regarding the ANFIS-FFA (the superior model) is presented in the following Box.

```
%% Cd calculation using developed ANFIS-FFA model
clc
clearall
closeall
%% Read data
Prompt={'F1','b/B','b/y1','p/y1'};
      Title='Enter the values of input variables';
DefaultValues={'[1;1;1]','[1;1;1]','[1;1;1]','[1;1;1]'};
PARAMS=inputdlg(Prompt,Title,3,DefaultValues);
F1=str2num(PARAMS{1}); bB=str2num(PARAMS{2});
by1=str2num(PARAMS{3});py1=str2num(PARAMS{4});
if length(F1)<2
   a1=[F1;F1];a2=[bB;bB];a3=[by1;by1];a4=[py1;py1];
else
   a1=F1;a2=bB;a3=by1;a4=py1;
end
TestInputs=[a1 a2 a3 a4]; z=length(F1);TestTargets=ones(z,1);
data.TestInputs=TestInputs;data.TestTargets=TestTargets;
x=data.TestInputs;t=data.TestTargets;
%% FIS generation using FCM method
fis=genfis3(x,t,'sugeno',7);clc
%% Replace the optimized values with initial parameters
% Inputs
fis.input(1).mf(1).params = [0.0565 0.3372];
fis.input(1).mf(2).params = [0.0491 0.3154];
fis.input(1).mf(3).params = [0.0565 0.3445];
fis.input(1).mf(4).params = [0.0589 0.4242];
fis.input(1).mf(5).params = [0.0898 0.5993];
fis.input(1).mf(6).params = [0.0221 0.3065];
fis.input(1).mf(7).params = [0.0582 0.4709];
fis.input(2).mf(1).params = [0.1101 0.3798];
fis.input(2).mf(2).params = [0.2385 0.8831];
fis.input(2).mf(3).params = [0.2492 0.3101];
fis.input(2).mf(4).params = [0.2510 1.4497];
fis.input(2).mf(5).params = [0.2304 1.4480];
fis.input(2).mf(6).params = [0.2291 1.4518];
fis.input(2).mf(7).params = [0.1944 1.4633];
fis.input(3).mf(1).params = [0.6593 0.8380];
fis.input(3).mf(2).params = [0.6036 1.8200];
fis.input(3).mf(3).params = [0.6542 0.7039];
fis.input(3).mf(4).params = [0.6545 3.3151];
fis.input(3).mf(5).params = [1.1921 5.2741];
fis.input(3).mf(6).params = [0.6150 2.7989];
fis.input(3).mf(7).params = [0.8215 4.1118];
fis.input(4).mf(1).params = [0.1354 0.6260];
fis.input(4).mf(2).params = [0.1056 0.5572];
fis.input(4).mf(3).params = [0.1353 0.6574];
fis.input(4).mf(4).params = [0.0879 0.7914];
fis.input(4).mf(5).params = [0.0573 0.6414];
fis.input(4).mf(6).params = [0.0744 0.6661];
fis.input(4).mf(7).params = [0.0754 0.7613];
% Outputs
fis.output.mf(1).params = [-1.1236  3.9461 -0.0381 -1.1479 -1.0373];
fis.output.mf(2).params = [-0.6988 -0.0093  0.0508 -0.3334  0.8788];
fis.output.mf(3).params = [-1.5878 -2.3045  0.2272 -0.8025  3.0169];
fis.output.mf(4).params = [ 0.6068  0.0837  0.0300  0.6199 -0.3656];
fis.output.mf(5).params = [ 0.0308  0.0567 -0.0204  0.1020  0.4216];
fis.output.mf(6).params = [-1.0323 -0.0789  0.0803  0.5576  0.3392];
fis.output.mf(7).params = [ 2.3300 -1.0774  0.1090 -1.8136  1.8717];
%% Cd calculation
Cd=abs(evalfis(data.TestInputs,fis))
```

Box A1. MATLAB code for the estimation DC.

References

Abdollahi A., Kabiri-Samani A., Asghari K., Atoof H., Bagheri S., Numerical modeling of flow field around the labyrinth side-weirs in the presence of guide vanes, ISH Journal of Hydraulic Engineering 23 (2017) 71-79.

Abdulshahed A.M., Longstaff A.P., Fletcher S., The application of ANFIS prediction models for thermal error compensation on CNC machine tools, Applied Soft Computing 27 (2015) 158-168.

Ameri M., Dehghani A.A., Ahmadi A., Elementary discharge coefficient of a triangular–rectangular sharp-crested side weir in subcritical flow, International Journal of River Basin Management 14 (2016) 95-102.

Aydin M. C., Investigation of a sill effect on rectangular side-weir flow by using CFD, Journal of Irrigation and Drainage Engineering 142 (2015) 04015043.

Aydin M.C., New approach for estimation of rectangular side weirs discharge in subcritical flow, Journal of Irrigation and Drainage Engineering 142 (2016) 04016012.

Aydin M.C., Emiroglu M.E., Determination of capacity of labyrinth side weir by CFD, Flow Measurement and Instrumentation 29 (2013) 1-8.

Aydin M.C., Emiroglu M.E., Numerical analysis of subcritical flow over two-cycle trapezoidal labyrinth side weir, Flow Measurement and Instrumentation 48 (2016) 20-28.

Aydin M.C., Öztürk M., Yücel A., Experimental and numerical investigation of self-priming siphon side weir on a straight open channel, Flow Measurement and Instrumentation 45 (2015) 140-150.

Azamathulla H.M., Haghiabi A.H., Parsaie A., Prediction of side weir discharge coefficient by support vector machine technique, Water Science and Technology: Water Supply 16 (2016) 1002-1016.

Azimi H., Shabanlou S., The flow pattern in triangular channels along the side weir for subcritical flow regime, Flow Measurement and Instrumentation 46 (2015) 170-178.

Azimi H., Shabanlou S., U-shaped channels along the side weir for subcritical and supercritical flow regimes, ISH Journal of Hydraulic Engineering (2018) 1-11.

Azimi H., Bonakdari H., Ebtehaj I., Sensitivity analysis of the factors affecting the discharge capacity of side weirs in trapezoidal channels using extreme learning machines, Flow Measurement and Instrumentation 54 (2017) 216-223.

Azimi H., Bonakdari H., Ebtehaj I., Michelson D.G.A., combined adaptive neuro-fuzzy inference system–firefly algorithm model for predicting the roller length of a hydraulic jump on a rough channel bed, Neural Computing and Applications 29 (2018a) 249-258.

Azimi H., Bonakdari H., Ebtehaj I., Gharabaghi B., Khoshbin F., Evolutionary design of generalized group method of data handling-type neural network for estimating the hydraulic jump roller length, ActaMechanica 229 (2018b) 1197-1214.

Azimi H., Shabanlou S., Salimi M.S., Free surface and velocity field in a circular channel along the side weir in supercritical flow conditions, Flow Measurement and Instrumentation 38 (2014) 108-115.

Azimi H., Shabanlou S., Ebtehaj I., Bonakdari H., Kardar S., Combination of computational fluid dynamics, adaptive neuro-fuzzy inference system, and genetic algorithm for predicting discharge coefficient of rectangular side orifices, Journal of Irrigation and Drainage Engineering 143 (2017) 04017015.

Bagheri S., Kabiri-Samani A. R., Heidarpour M., Discharge coefficient of rectangular sharp-crested side weirs, Part I: traditional weir Eq., Flow Measurement and Instrumentation 35 (2014) 109-115.

Chatterjee S., Mahapatra S.S., Lamberti L., Pruncu C.I., Prediction of welding responses using AI approach: adaptive neuro-fuzzy inference system and genetic programming, Journal of the Brazilian Society of Mechanical Sciences and Engineering 44 (2022) 1-15.

Crispino G., Cozzolino L., Della Morte R., Gisonni C., Supercritical low-crested bilateral weirs: hydraulics and design procedure, Journal of Applied Water Engineering and Research 3 (2015) 35-42.

Dursun O.F., Kaya N., Firat M., Estimating discharge coefficient of semi-elliptical side weir using ANFIS, Journal of hydrology 426 (2012) 55-62.

Ebtehaj I., and Bonakdari H., Assessment of evolutionary algorithms in predicting non-deposition sediment transport, Urban Water Journal 13 (2016) 499-510.

Ebtehaj I., Bonakdari H., Khoshbin F., Azimi H., Pareto genetic design of group method of data handling type neural network for prediction discharge coefficient in rectangular side orifices, Flow Measurement and Instrumentation 41 (2015) 67-74.

Ebtehaj I., Bonakdari H., Shamshirband S., Ismail Z., Hashim R., New approach to estimate velocity at limit of deposition in storm sewers using vector machine coupled with firefly algorithm, Journal of Pipeline Systems Engineering and Practice 8 (2017) 04016018.

Ebtehaj I., Bonakdari H., A support vector regression-firefly algorithm-based model for limiting velocity prediction in sewer pipes, Water Science and Technology 73 (2016) 2244-2250.

Emiroglu M.E., Bilhan O., Kisi O., Neural networks for estimation of discharge capacity of triangular labyrinth side-weir located on a straight channel, Expert Systems with Applications 38 (2011) 867-874.

Emiroglu M.E., Gogus M., Tunc M., Islamoglu K., Effects of Antivortex Structures Installed on Trapezoidal Labyrinth Side Weirs on Discharge Capacity and Scouring, Journal of Irrigation and Drainage Engineering 143 (2017) 04017006.

Ferreira C.V., Biesek F.L., Scalice R.K., Product innovation management model based on manufacturing readiness level (MRL), design for manufacturing and assembly (DFMA) and technology readiness level (TRL), Journal of the Brazilian Society of Mechanical Sciences and Engineering 43 (2021) 1-18.

Freitas F.A., Jafelice R.M., Silva J.W.D., Rabelo D.D.S., Nomelini Q.S.S., Moura J.D.R.V.D., Ramos J.E., A new data normalization approach applied to the electromechanical impedance method using adaptive neuro-fuzzy inference system, Journal of the Brazilian Society of Mechanical Sciences and Engineering 43 (2021) 1-13.

Gholami A., Bonakdari H., Ebtehaj I., Mohammadian M., Gharabaghi B., Khodashenas S.R., Uncertainty analysis of intelligent model of hybrid genetic algorithm and particle swarm optimization with ANFIS to predict threshold bank profile shape based on digital laser approach sensing, Measurement 121 (2018) 294-303

Goldberg D.E., Holland J.H., Genetic algorithms and machine learning. Machine learning 3 (1988) 95-99.

Granata F., Gargano R., Santopietro S., A flow field characterization in a circular channel along a side weir. Flow Measurement and Instrumentation 52 (2016) 92-100.

Jang J.S., ANFIS: adaptive-network-based fuzzy inference system, IEEE Transactions on Systems, Man, and Cybernetics 23 (1993) 665-685.

Karimi M., Attari J., Saneie M., JaliliGhazizadeh M.R., Side Weir Flow Characteristics: Comparison of Piano Key, Labyrinth, and Linear Types, Journal of Hydraulic Engineering 144 (2018) 04018075.

Kennedy R., Particle swarm optimization, In Proceedings of IEEE International Conference on Neural Networks IV Vol. 1000 (1995) p. 33.

Khameneh H.Z., Khodashenas S.R., Esmaili K., The effect of increasing the number of cycles on the performance of labyrinth side weir, Flow Measurement and Instrumentation 39 (2014) 35-45.

Khoshbin F., Bonakdari H., Ashraf Talesh S.H., Ebtehaj I., Zaji A.H., Azimi H., Adaptive neuro-fuzzy inference system multi-objective optimization using the genetic algorithm/singular value decomposition method for modelling the discharge coefficient in rectangular sharp-crested side weirs, Engineering Optimization 48 (2016) 933-948.

Kisi O., Emiroglu M.E., Bilhan O., Guven A., Prediction of lateral outflow over triangular labyrinth side weirs under subcritical conditions using soft computing approaches, Expert systems with Applications 39 (2012) 3454-3460.

Mahmodinia S., Javan M., Eghbalzadeh A., The effects of side-weir height on the free surface turbulent flow, KSCE Journal of Civil Engineering 18 (2014) 2244-2251.

Novak G., Steinman F., Müller M., Bajcar T., Study of velocity field at model sideweir using visualization method, Journal of Hydraulic Research 50 (2012) 129-133.

Onen F., Agaccioglu H., Live bed scour at a side-weir intersection located on an alluvial channel. Irrigation and Drainage 62 (2013) 488-500.

Paris E., Solari L., Bechi G., Applicability of the De Marchi hypothesis for side weir flow in the case of movable beds, Journal of Hydraulic Engineering 138 (2012) 653-656.

Parsaie A., Haghiabi A., The effect of predicting discharge coefficient by neural network on increasing the numerical modeling accuracy of flow over side weir, Water resources management 29 (2015) 973-985.

Parsaie A., Yonesi H., Najafian S., Prediction of flow discharge in compound open channels using adaptive neuro fuzzy inference system method, Flow Measurement and Instrumentation 54 (2017) 288-297.

Qasem N.M., Ebtehaj I., Bonakdari H., Potential of radial basis function network with particle swarm optimization for prediction of sediment transport at the limit of deposition in a clean pipe, Sustainable Water Resources Management 3 (2017) 391-401.

Roushangar K., Khoshkanar R., Shiri J., Predicting trapezoidal and rectangular side weirs discharge coefficient using machine learning methods, ISH Journal of Hydraulic Engineering 22 (2016) 254-261.

Sai T., Pathak V.K., Srivastava A.K., Modeling and optimization of fused deposition modeling (FDM) process through printing PLA implants using adaptive neuro-fuzzy inference system (ANFIS) model and whale optimization algorithm, Journal of the Brazilian Society of Mechanical Sciences and Engineering 42 (2020) 1-19.

Shafiei S., Najarchi M., Shabanlou S., A novel approach using CFD and neuro-fuzzy-firefly algorithm in predicting labyrinth weir discharge coefficient, Journal of the Brazilian Society of Mechanical Sciences and Engineering 42 (2020) 1-19.

Shaghaghi S., Bonakdari H., Gholami A., Ebtehaj I., Zeinolabedini M., Comparative analysis of GMDH neural network based on genetic algorithm and particle swarm optimization in stable channel design, Applied Mathematics and Computation 313 (2017) 271-286.

Shihabudheen K.V., Pillai G.N., Recent advances in neuro-fuzzy system: A survey, Knowledge-Based Systems 152 (2018) 136-162.

Yang X.S., Firefly algorithm, Nature-inspired metaheuristic algorithms 20 (2008) 79-90.

Yaseen Z.M., Ebtehaj I., Bonakdari H., Deo R.C., Mehr A.D., Mohtar W.H.M.W., Diop L., El-shafie A., Singh V.P., Novel approach for streamflow forecasting using a hybrid ANFIS-FFA model, Journal of Hydrology 554C (2017) 263-276.

Yaseen Z.M., Ghareb M.I., Ebtehaj I., Bonakdari H., Siddique R., Heddam S., Yusif A., Deo R., Rainfall pattern forecasting using novel hybrid intelligent model based ANFIS-FFA, Water Resources Management 32 (2018) 105-122.

Zahiri A., Azamathulla H.M., Bagheri S., Discharge coefficient for compound sharp crested side weirs in subcritical flow conditions, Journal of hydrology 480 (2013) 162-166.